Mathematical Biosciences 355 (2023) 108940

Contents lists available at ScienceDirect

Mathematical Biosciences

journal homepage: www.elsevier.com/locate/mbs

Original Research Article

A hybrid spatiotemporal model of PCa dynamics and insights into optimal therapeutic strategies

Andrew Burbanks [a], Marianna Cerasuolo [a,*], Roberto Ronca [b], Leo Turner [a]

[a] School of Mathematics and Physics, University of Portsmouth, Lion Gate Building, Lion Terrace, Portsmouth, PO1 3HF, Hampshire, United Kingdom
[b] Experimental Oncology and Immunology, Department of Molecular and Translational Medicine, University of Brescia, Viale Europa 11, Brescia, 25123, Italy

ARTICLE INFO

MSC:
92C50
37N25

Keywords:
Prostate cancer
Mathematical model
Hybrid cellular automaton
Chemotherapy
Drug resistance

ABSTRACT

Using a hybrid cellular automaton with stochastic elements, we investigate the effectiveness of multiple drug therapies on prostate cancer (PCa) growth. The ability of Androgen Deprivation Therapy to reduce PCa growth represents a milestone in prostate cancer treatment, nonetheless most patients eventually become refractory and develop castration-resistant prostate cancer. In recent years, a "second generation" drug called enzalutamide has been used to treat advanced PCa, or patients already exposed to chemotherapy that stopped responding to it. However, tumour resistance to enzalutamide is not well understood, and in this context, preclinical models and *in silico* experiments (numerical simulations) are key to understanding the mechanisms of resistance and to assessing therapeutic settings that may delay or prevent the onset of resistance. In our mathematical system, we incorporate cell phenotype switching to model the development of increased drug resistance, and consider the effect of the micro-environment dynamics on necrosis and apoptosis of the tumour cells. The therapeutic strategies that we explore include using a single drug (enzalutamide), and drug combinations (enzalutamide and everolimus or cabazitaxel) with different treatment schedules. Our results highlight the effectiveness of alternating therapies, especially alternating enzalutamide and cabazitaxel over a year, and a comparison is made with data taken from TRAMP mice to verify our findings.

1. Introduction

Prostate cancer (PCa) is the second most common cause of cancer among men worldwide [2,3], accounting for 26% of all new cancer cases in males in the UK as of 2016 [4], and with more than 11,500 men dying with PCa every year [5], research into the causes of prostate cancer, and potential therapies, remains critical. The prostate is a small organ found immediately below the bladder that manufactures and secretes seminal fluid, and maintaining the prostate in good order is essential for optimal urinary health and sexual vitality [6]. The development of prostate tumours is heavily dependent on the presence of androgens (the male sex hormones), and as such the inhibition of androgen signalling either by depriving the tumour of androgen or by blocking the activity of the relevant receptors has led to the use of androgen deprivation therapy (ADT) as the most common treatment for advanced PCa [7,8]. While ADT is effective for most patients [9] at controlling PCa for between 15 and 18 months [10], clinical studies have shown that the majority of prostate tumours will begin to show signs of growth after this period [11], leading to castration-resistant prostate cancer (CRPC) for which the patient has an average survival period of two to three years. Alternative methods of treatment are currently provided for PCa in the UK [12], including chemotherapy, steroid therapy and radiotherapy.

Over the past few decades mathematical models of tumour growth have been implemented and fitted to experimental and/or clinical data in order to better understand this disease, to formulate new hypotheses, to make predictions, and to guide new experiments and clinical trials in an effort to obtain personalised cancer treatments [13]. *In silico* experiments allow us to consider multiple hypotheses and to test the effect of different treatments on cancer progression without the ethical issue of not providing the right treatment to patients [14]. In this work, we will use a newly developed mathematical model to focus on the effectiveness of different chemotherapy regimes and their impact upon PCa cellular differentiation.

Cerasuolo et al. [1] developed a stochastic differential equation (SDE) model that used the experimental evidence and collected data from the response of TRAMP mice (a multistage transgenic mouse model that mimics the onset and progression of PCa) to enzalutamide, both *in vivo* and *in vitro*, to describe the tumour's response to enzalutamide and subsequent relapse. As part of the study *in silico* experiments showed that, under any length of treatment schedule, enzalutamide-resistant cells become the dominant phenotype, suggesting that these

* Corresponding author.
E-mail address: marianna.cerasuolo@port.ac.uk (M. Cerasuolo).

https://doi.org/10.1016/j.mbs.2022.108940
Received 15 May 2022; Received in revised form 9 November 2022; Accepted 9 November 2022
Available online 15 November 2022

cells have a higher fitness than sensitive cells, meaning that they are able to grow more efficiently under oxygen- and glucose-deprived conditions. While the model considers TRAMP mice, we note that PCa in TRAMP mice mimics the development of human PCa, as well as reacting and relapsing in response to ADT in a manner similar to that observed in men [15].

One limitation of the SDE approach is that it lacks a representation of the spatial distribution of cell types, which can make comparison to real world data difficult (e.g. results from non-invasive imaging tests such as MRI scans [16]). Incorporating this concept can be achieved by using either a continuum model, a cellular automaton (CA) or a hybrid approach. While continuum models have been used extensively to consider many different elements of tumour growth and treatment [17–20], CA models are considered more efficient to use due to computational ease and the ability to provide qualitative information without needing exact parameter values [21–25]. However, as the behaviours of the PCa cells and the various chemicals occur on different time scales, we consider a multi-scale model. This leads to a hybrid approach, in which partial differential equations (PDEs) govern the behaviour of the drugs and other chemicals (over the 'fast' timescale), and a CA provides the rules for the dynamics of the tumour cells (over the 'slow' timescale). Hybrid approaches have been used to consider avascular tumour growth [22], immune cell response [26], and radiotherapy in PCa [27]. The novelty of this model comes from considering the effects of multiple drug therapies, combined with modelling the spatial distributions of cell-types and chemicals, and in the use of probability functions informed by the previously developed SDE, in formulating the CA rules to govern the behaviour of the tumour cells. We also incorporate asymmetric cell division [28,29] to represent the spontaneous development of mutations.

1.1. Overview

In Section 2 we give the formulation of the hybrid model, incorporating the PDEs that model chemical interactions in the micro-environment (Section 2.1) and the stochastic CA rules that govern cell behaviour (Section 2.2), paying particular attention to the functions used to model the probabilities of certain cell-level events. Section 2.3 provides a brief overview of the therapies that will be considered.

In Section 3, we describe the simulation process used for the hybrid model and indicate how the various drug therapies are implemented. Table A.1 provides details of the experimental parameters and the sources from which they were obtained. In Section 4 we describe the results of our simulations and their robustness, and compare the performance of the various therapies in the model. We conclude with a discussion (Section 5) of the implications of our findings and suggest further improvements to the model.

2. Model formulation

For this model we consider a tumour that has three populations of cell phenotypes: one PCa cell phenotype sensitive to the chemotherapy drug enzalutamide, S_i, another resistant to it, R_i, and the necrotic cells, N. We consider that each tumour cell phenotype will go through a proliferating phase (subscript p) and a quiescent phase (subscript q), with different behaviour for each phase. While the cell behaviour will be governed by the rules of the CA described below, the micro-environment consisting of oxygen, glucose, hydrogen ions and cancer drugs will be modelled using a system of PDEs. We do not consider androgen as a limiting factor on the growth of the tumour, as we assume that the tumour is not also undergoing ADT.

This model simulates a two dimensional slice through a tumour and surrounding tissue, with a boundary region intended to simulate the local vasculature that delivers nutrients and the selected drugs into the region by diffusion, and excretes waste products such as hydrogen ions. To do this we consider a square spatial domain, Ω, which has been partitioned into a regular grid of 100×100 sites (or points) with a boundary region occupying the outermost ring of sites. Each site represents a region in the slice of tissue measuring 20 μm × 20 μm in size, chosen to have approximately the same area as a tumour cell [30]. The interior sites are each occupied by one of six cell types; S_p, S_q, R_p, R_q, N, and healthy prostate cells, P. The healthy prostate cells are considered to have little to no effect on the micro-environment when compared to the PCa cells, and are assumed to undergo apoptosis as the tumour grows, allowing the tumour to expand unhindered.

2.1. Micro-environment

The micro-environment is defined to be the filled space around a cell with which only that cell interacts. The chemicals considered in the model are oxygen, O, glucose, G, and hydrogen ions, H, as they have a key role in cell growth either as nutrients or inhibitors. We assume that O, G, and H behave as shown by Ibrahim-Hashim et al. [31] and Robertson-Tessi et al. [30], with the relevant parameter values dependent on the cell type present at the corresponding site, where we assume that necrotic cells do not consume O or G, and do not produce H.

The supplemental information for [30] considers that cells metabolise oxygen and glucose to produce adenosine triphosphate (ATP), which is the primary source of energy for cellular behaviour, and that there are two mechanisms for ATP production: the glycolytic pathway, which is less efficient but does not require oxygen, and the aerobic respiration pathway, which does require oxygen and is roughly eighteen times more efficient than the glycolytic pathway. Under ideal conditions a cell will use the aerobic pathway exclusively. However, if oxygen becomes scarce the cell will temporarily increase usage of the glycolytic pathway in an attempt to mitigate the decrease in ATP production, and if oxygen becomes absent then the glycolytic pathway is used exclusively. A side effect of over-usage of the glycolytic pathway is an acidification of the extracellular pH, which is caused by the final by-product of the glycolytic pathway, lactic acid, being excreted into the micro-environment. This can be detrimental to cell survival. However, some tumour cells show a higher adaptability to acidic environments, especially enzalutamide-resistant PCa cells, which perform much better (with higher fitness) in a more acidic environment than enzalutamide-sensitive PCa or healthy prostate cells [1].

When glucose is depleted, the cell must either use alternative sources of energy or reduce its ATP requirements by becoming quiescent. As this model does not consider other energy sources, the cells are assumed to become quiescent when ATP production drops below a threshold, and then to undergo apoptosis if a minimal ATP need is not met.

To discuss the functional forms used to model the activity of the respective chemicals, Robertson-Tessi et al. [30] considered the important steps of metabolism which use several intermediate chemicals not actively modelled, such as nicotinamide adenine dinucleotide (NAD^+), its reduced form (NADH) and pyruvate (Pyr), which is the chemical used in both the aerobic and anaerobic pathways.

We assume that the ratio of the concentration of NAD^+ to that of its reduced form remains relatively constant over long time periods, and that ATP is well regulated under the conditions modelled. The final assumption for the internal metabolism is that pyruvate remains stable over time, as it is not exported from the cell. This allows us to consider the temporal derivatives of these intermediate products to be zero, and thus the cell is treated as a closed system, except for the inputs of oxygen and glucose and the excretion of hydrogen ions, for the purpose of modelling the internal metabolism.

2.1.1. Cell metabolism model equations

All equations presented in this section are well established equations for cellular metabolism, and were developed by Robertson-Tessi et al. in 2015 [30]. The diffusion and consumption of oxygen, $O(\mathbf{x},t)$, is modelled using the reaction–diffusion equation:

$$\frac{\partial O(\mathbf{x},t)}{\partial t} = D_O \nabla^2 O(\mathbf{x},t) - V_O \frac{O(\mathbf{x},t)}{O(\mathbf{x},t)+k_O}, \tag{1}$$

where D_O denotes the diffusion coefficient, V_O denotes the maximum oxygen consumption under ideal conditions and k_O is the half-maximum consumption for the Michaelis–Menten kinetics, with parameter values dependent on the cell type present at the position $\mathbf{x}$. Assuming that normal ATP demand is satisfied when the oxygen concentration is high enough to ensure that

$$-V_O \frac{O(\mathbf{x},t)}{O(\mathbf{x},t)+k_O} \approx -V_O, \tag{2}$$

we assume that the target normal ATP production is given [30] by

$$A_O = \frac{29 V_O}{5}. \tag{3}$$

Glucose consumption is driven to satisfy the normal ATP demand, and as such is given by:

$$\frac{\partial G(\mathbf{x},t)}{\partial t} = D_G \nabla^2 G(\mathbf{x},t) - \left(\frac{p_G A_O}{2} - \frac{27 V_O \frac{O(\mathbf{x},t)}{O(\mathbf{x},t)+k_O}}{10} \right) \frac{G(\mathbf{x},t)}{G(\mathbf{x},t)+k_G}, \tag{4}$$

where D_G is the diffusion coefficient, p_G is the multiplier representing the altered glucose metabolism of the tumour cells, and k_G is the half-maximum of the Michaelis–Menten kinetics, which was introduced to stop high glucose consumption when the concentration was low. The fraction $\frac{27}{10}$ is included to recognise that from five oxygen molecules there are 27 ATP molecules produced under ideal conditions, with the additional factor of a half included to reflect that each glucose molecule is guaranteed to produce a minimum of two ATP molecules [30]. As with glucose, the parameter values are dependent on the cell type present at the position $\mathbf{x}$.

Hydrogen regulation involves a proportional relationship between anaerobic glucose consumption and the extracellular concentration of hydrogen, and is given by:

$$\frac{\partial H(\mathbf{x},t)}{\partial t} = D_H \nabla^2 H(\mathbf{x},t) + k_H \left(\frac{29 \left(p_G V_O - V_O \frac{O(\mathbf{x},t)}{O(\mathbf{x},t)+k_O} \right)}{5} \right), \tag{5}$$

where D_H is the diffusion coefficient, p_G is the altered glucose metabolism multiplier seen in many tumour cells, and k_H accounts for proton buffering (meant as the capacity to contain pH lowering) caused by sodium bicarbonate and other physiological buffer systems present *in vivo*. When the oxygen concentration is sufficient to allow maximum aerobic respiration the net hydrogen production is zero for the normal phenotype, while when there is no aerobic respiration the hydrogen production rate will be roughly twice the glucose consumption. As we consider $p_G > 1$ for the PCa cells, i.e., we assume both tumour cell phenotypes to be glycolytic at some level, there will always be some hydrogen production, regardless of oxygen consumption.

Finally we consider the ATP dynamics, in which the production is determined by the nutrient consumption rates, that is

$$\begin{aligned} \frac{\partial A(\mathbf{x},t)}{\partial t} &= D_A \nabla^2 A(\mathbf{x},t) + 2 \left(\frac{p_G A_O}{2} - \frac{27 V_O \frac{O(\mathbf{x},t)}{O(\mathbf{x},t)+k_O}}{10} \right) \frac{G(\mathbf{x},t)}{G(\mathbf{x},t)+k_G} \\ &\quad + \frac{27 V_O \frac{O(\mathbf{x},t)}{O(\mathbf{x},t)+k_O}}{5}, \end{aligned} \tag{6}$$

The ATP value is used to determine whether cells switch between the proliferating and quiescent phase, and whether apoptosis occurs.

2.1.2. Drug therapy model equations

The drugs introduced in the therapies of this model are enzalutamide, Ez, cabazitaxel, Cb, and everolimus, Ev. Enzalutamide is a non-steroidal androgen receptor inhibitor that has been approved for the treatment of CRPC [32], although notably PCa progression is eventually seen in patients, and PCa resistance to enzalutamide has also been noted. At this time, the mechanism that governs this resistance has not been discovered [33]. Cabazitaxel is a next generation taxane, a type of drug used widely for chemotherapy, that works by impairing the natural dynamics of microtubules, which provide shape and structure to eukaryotic cells, blocking mitosis and subsequently leading to apoptosis [34]. It has been approved for treatment when PCa progression has occurred during treatment with docetaxel [35], although it has been used alone in clinical trials [36]. Everolimus is an mTOR inhibitor (mTOR is the pathway that regulates all major cellular processes such as cell growth, proliferation and protein synthesis) and is involved in several clinical trials evaluating combinations of drugs as potential therapeutic strategies [37]. The PDEs for the drugs can be written as:

$$\begin{aligned} \frac{\partial \mathrm{Ez}(\mathbf{x},t)}{\partial t} &= D_{\mathrm{Ez}} \nabla^2 \mathrm{Ez}(\mathbf{x},t), \\ \frac{\partial \mathrm{Cb}(\mathbf{x},t)}{\partial t} &= D_{\mathrm{Cb}} \nabla^2 \mathrm{Cb}(\mathbf{x},t), \\ \frac{\partial \mathrm{Ev}(\mathbf{x},t)}{\partial t} &= D_{\mathrm{Ev}} \nabla^2 \mathrm{Ev}(\mathbf{x},t), \end{aligned} \tag{7}$$

where the D_i (for $i = \mathrm{Ez}, \mathrm{Cb}, \mathrm{Ev}$) are the constant diffusion coefficients for the respective drugs, and as such we assume that the drugs are unhindered by the type of cell they are diffusing around. We also assume that the drugs are only effective against proliferating cells, due to their increased metabolic activity over quiescent cells. Finally, the degradation of the drugs is assumed to occur in the vasculature between doses, rather than in the tissue level, and as such the degradation term is included in the boundary condition for the tissue region. Hence, these Eqs. (7) are a simplified version of the drug equations considered by Hamis et al. [38] in which drug decay appears explicitly.

2.1.3. Micro-environment model equations and parameters

From the above, we consider the micro-environment to be governed by the following system of PDEs:

$$\begin{aligned} \frac{\partial c(\mathbf{x},t)}{\partial t} &= D_c \nabla^2 c(\mathbf{x},t) + g_c \quad c = O, G, H, A \\ \frac{\partial \mathrm{j}(\mathbf{x},t)}{\partial t} &= D_{\mathrm{j}} \nabla^2 \mathrm{j}(\mathbf{x},t) \qquad j = \mathrm{Ez}, \mathrm{Cb}, \mathrm{Ev}, \end{aligned} \tag{8}$$

with

$$\begin{aligned} g_O &= -V_O \frac{O(\mathbf{x},t)}{O(\mathbf{x},t)+k_O}, \qquad g_G = -\left(\frac{p_G A_O}{2} + \frac{27}{10} g_O \right) \frac{G(\mathbf{x},t)}{G(\mathbf{x},t)+k_G}, \\ g_H &= k_H \left(\frac{29 \left(p_G V_O + g_O \right)}{5} \right), \; g_A = -\left(2 g_G + \frac{27 g_O}{5} \right) \end{aligned} \tag{9}$$

with parameter values dependent on the cell type present. All of the micro-environment equations are assumed to have Dirichlet boundary conditions:

$$\begin{aligned} &O(\mathbf{x},t) = 0.014 \text{ mMol}/\ell, \qquad G(\mathbf{x},t) = 0.05 \text{ mMol}/\ell, \\ &H(\mathbf{x},t) = 7.2 \text{ pH}, \qquad A(\mathbf{x},t) = 1 \text{ mMol}/\ell, \\ &\mathrm{Ez}(\mathbf{x},t) = f_{\mathrm{Ez}}(t), \;\; \mathrm{Cb}(\mathbf{x},t) = f_{\mathrm{Cb}}(t), \;\; \mathrm{Ev}(\mathbf{x},t) = f_{\mathrm{Ev}}(t), \end{aligned} \tag{10}$$

for all $\mathbf{x} \in \partial\Omega$. In TRAMP mice enzalutamide is given orally (3 mg/kg in the drinking water) daily. The dosage and its consumption are such that the effective concentration in the vasculature fluctuates so minutely as to be considered constant, which the model readily assumes. Cabazitaxel is administered by intraperitoneal injection, that is direct injection into the body cavity, in a much larger dose once (15 mg/kg) every fortnight, and 1 mg/kg of everolimus is given every

other day by intraperitoneal injection. The model assumes an adaptive therapy for the drugs, where the amount of drug provided is such that the total drug concentration in the blood flow does not exceed the target quantity. Therefore, when the new cycle starts the maximum drug concentration in the body will be the one indicated in (13) for enzalutamide, in (14) for cabazitaxel, and in (15) for everolimus.

As the drugs do not immediately leave the vasculature when the doses stop, we assume that the drug degradation occurs in the vasculature. Therefore the change in drug concentration in the vasculature is given by

$$\dot{D} = -\eta_D D(t), \tag{11}$$

which can be solved to give

$$D = D(0)e^{-\eta_D t}, \tag{12}$$

and therefore we consider an exponential term for the degradation rate in the boundary conditions of the drugs.

To reflect the dose and timings of each drug, we consider the boundary condition for each drug to be a function of time. In the first seven weeks of tumour growth the boundary conditions for the drugs are initially set to zero, as we assume that no treatment is given before the tumour is "visible". Subsequently, the enzalutamide boundary function $f_{\mathrm{Ez}}(t)$ is given by

$$f_{\mathrm{Ez}}(t) = \begin{cases} \mathrm{Ez}^* & \text{if} \quad t \in [t_i, t_j], \\ \mathrm{Ez}^* e^{-\eta_{\mathrm{Ez}}(t-t_j)} & \text{if} \quad t > t_j, \end{cases} \tag{13}$$

where Ez^* is the administered dose over a day, η_{Ez} is the degradation rate, t_i are the start times for giving the doses of enzalutamide, t_j are the stop times for finishing the course of dosages, $i < j$ and $i, j \in J$, where J is the set of start and stop dates of the given therapy.

The cabazitaxel boundary condition is given by

$$f_{\mathrm{Cb}}(t) = \begin{cases} \mathrm{Cb}^* & \text{if} \quad t = t^i_{\mathrm{Cb}}, \\ \mathrm{Cb}^* e^{-\eta_{\mathrm{Cb}}(t-t^i_{\mathrm{Cb}})} & \text{if} \quad t^i_{\mathrm{Cb}} < t < t^{i+1}_{\mathrm{Cb}}, \end{cases} \tag{14}$$

where Cb^* is the administered dose over a day, η_{Cb} is the degradation rate and t^i_{Cb} is a start date, with $i \in I_c$, where I_c is the set of starting days for the selected therapy. Similarly, the everolimus boundary condition is

$$f_{\mathrm{Ev}}(t) = \begin{cases} \mathrm{Ev}^* & \text{if} \quad t = t^i_{\mathrm{Ev}}, \\ \mathrm{Ev}^* e^{-\eta_{\mathrm{Ev}}(t-t^i_{\mathrm{Ev}})} & \text{if} \quad t^i_{\mathrm{Ev}} < t < t^{i+1}_{\mathrm{Ev}}, \end{cases} \tag{15}$$

where Ev^* is the administered dose over a day, η_{Ev} is the degradation rate, t^i_{Ev} is a start date with $i \in I_e$, where I_e is the set of starting days for the selected therapy. An illustration of the boundary conditions used for each type of therapy is provided in Appendix B.

2.2. Cellular automata rules for the hybrid model

In this section we describe the CA rules for the PCa cell types S_p, S_q, R_p and R_q. Healthy cells and necrotic cells are assumed to remain unaffected throughout the simulation, and as such do not have CA rules assigned to them. For all rules we use $\mathbf{x}$ to denote the grid location for referencing the correct concentration of O, G and H, and the drugs, and the behaviour addressed by the rule occurs with the relevant probability $P(\mathbf{x})$ on each step [26]. Each CA iteration represents a single day, with each grid point being assessed once per iteration. Tumour cells follow the rules given below in order, only moving on to consider the next rule in the sequence if the checked behaviour does not happen, as illustrated in Fig. 1.

Parameter values used in Figs. 4–16 can be found in Table A.1. The probabilities that refer to drug-induced death are based on experiments and models developed in [1].

Necrosis. Necrosis is unplanned cell death that happens when the oxygen concentration becomes lower than a certain threshold, denoted by O_N. In the model it occurs with probability

$$P_{\mathrm{necro}} = \frac{1}{1 + e^{-k_N(O_N - O(\mathbf{x},t))}}, \tag{16}$$

(see Fig. 2(a)). Here k_N is the stiffness of the observed curve, with a larger k_N giving a sharper transition at the threshold [26]. If necrosis occurs, then the tumour cell becomes an N cell.

Apoptosis. Programmed cell death, apoptosis, occurs naturally when ATP total production, $A(\mathbf{x}, t)$, fails to reach a minimum threshold, ATP_d. Here we assume it occurs with probability

$$P_{\mathrm{apop}} = \frac{1}{1 + e^{-k_a(\mathrm{ATP}_d - A(\mathbf{x},t))}}, \tag{17}$$

(see Fig. 2(b)) with k_a as the stiffness of the curve [26].

Drug death. In [1] through *in vitro* experiments the authors showed that the drugs considered in this study affect the sensitive and resistant phenotype of the cells differently. Therefore, following results and models suggested in [1] for the death rates, we consider different functions governing the probability of death for each phenotype. For therapies where we administer multiple drugs, we compare the corresponding probabilities against a randomly generated number chosen uniformly in $[0, 1]$, and the cell dies if any of the probabilities are greater than the random number. As stated before, we assume that the chemotherapy drugs only interact with the proliferating cells, due to their increased activity and uptake rate compared to the quiescent cells.

Based on the work of Cerasuolo et al. [1] we hypothesise that S_p cell death by enzalutamide and cabazitaxel happens with the following probabilities:

$$\begin{aligned} P_{S-\mathrm{Enza}} &= \min\left[\delta_{\mathrm{Ez}}\mathrm{Ez}(\mathbf{x},t),\ 1\right], \\ P_{S-\mathrm{Caba}} &= \frac{\delta_{\mathrm{Cb}}\mathrm{Cb}(\mathbf{x},t)}{k_{\mathrm{Cb}} + \mathrm{Cb}(\mathbf{x},t)}, \end{aligned} \tag{18}$$

where δ_{Ez} and δ_{Cb} are the mortality rates, and k_{Cb} is the half-maximum coefficient for cabazitaxel.

For R_p cells cabazitaxel is more effective than enzalutamide [1], and so we use the following probabilities:

$$\begin{aligned} P_{R-\mathrm{Enza}} &= \frac{\lambda_{\mathrm{Ez}}\mathrm{Ez}(\mathbf{x},t)}{k_{\mathrm{Ez}} + \mathrm{Ez}(\mathbf{x},t)}, \\ P_{R-\mathrm{Caba}} &= \min\left[\lambda_{\mathrm{Cb}}\mathrm{Cb}(\mathbf{x},t), 1\right], \end{aligned} \tag{19}$$

where λ_{Ez} and λ_{Cb} are the mortality rates, and k_{Ez} is the half-maximum coefficient for enzalutamide (see Fig. 3(a) and Fig. 3(b)).

As for everolimus, while we assume that it is more effective than enzalutamide against R_p cells, there is insufficient evidence to assume that it has the linear death rate we have considered for cabazitaxel [1]. Therefore, for both cell phenotypes we consider a Michaelis–Menten dynamic [1], represented by

$$\begin{aligned} P_{S-\mathrm{Evero}} &= \frac{\delta_{\mathrm{Ev}}\mathrm{Ev}(\mathbf{x},t)}{k_{\mathrm{Ev}S} + \mathrm{Ev}(\mathbf{x},t)}, \\ P_{R-\mathrm{Evero}} &= \frac{\lambda_{\mathrm{Ev}}\mathrm{Ev}(\mathbf{x},t)}{k_{\mathrm{Ev}R} + \mathrm{Ev}(\mathbf{x},t)}, \end{aligned} \tag{20}$$

(see Fig. 3(c)) where δ_{Ev} and λ_{Ev} are the mortality rates, and $k_{\mathrm{Ev}S}$ and $k_{\mathrm{Ev}R}$ are the respective half-maximum coefficients.

It is important to observe that even if a cell population is resistant to a drug, it will still show some degree of sensitivity to that drug.

Proliferating to quiescent phase switch. As previously mentioned, cells can switch between the proliferating and quiescent phases based on their total ATP production. We consider the probability that a cell will become quiescent to be defined by

$$P_Q = \frac{1}{1 + e^{-k_q(\mathrm{ATP}_q - A(\mathbf{x},t))}}, \tag{21}$$

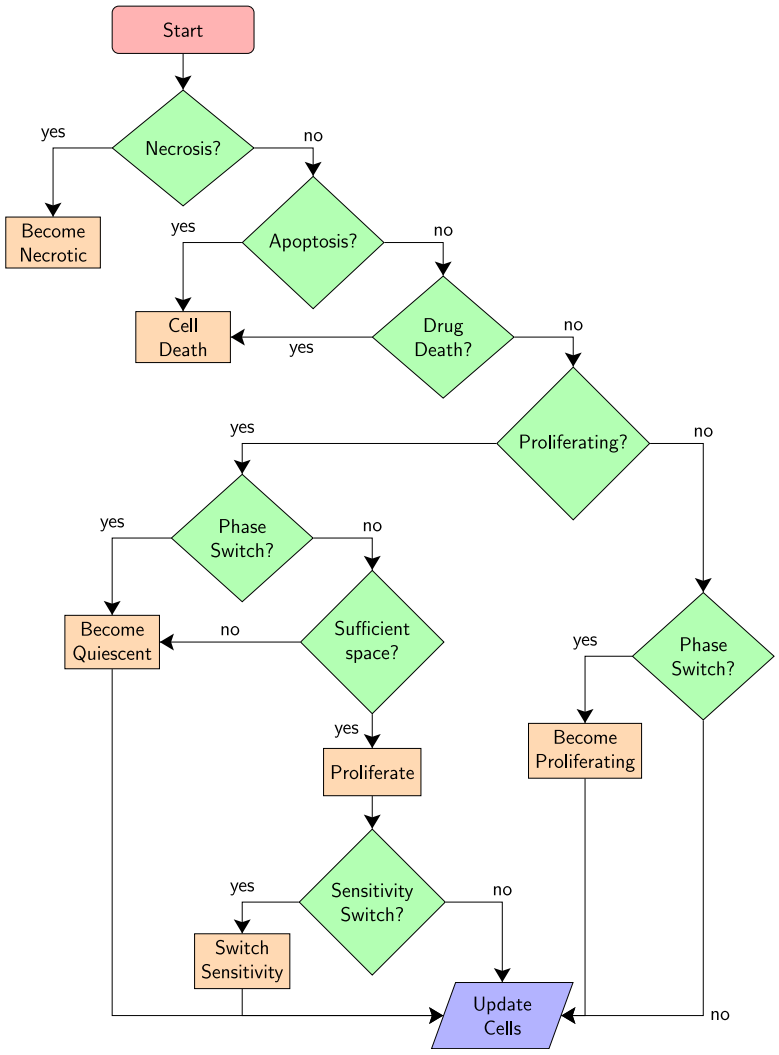

Fig. 1. A flowchart of one step in the life cycle of a PCa cell using the CA rules.

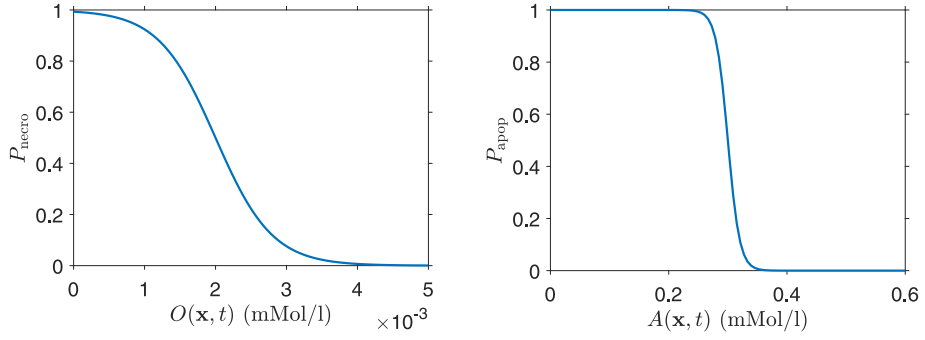

(a) Probability of necrosis. (b) Probability of apoptosis.

Fig. 2. Probability of necrosis and apoptosis occurring.

where ATP_q is the ATP production threshold for cells to remain proliferating. As PCa cells are either proliferating or quiescent we assume that the corresponding probability of becoming proliferating is given by

$$P_P = 1 - P_Q. \tag{22}$$

Proliferation. Proliferation is only considered for cells that did not undergo a phase switch within the current CA iteration. For the S_p and R_p cells to proliferate there must be a free (from tumour cells) neighbouring grid point in any of the four cardinal directions, and if this condition is met then proliferation occurs with probability

$$P_{Y-\text{Prolif}} = \min\left[1,\ K_Y p_{1Y}\left(\frac{O(\mathbf{x},t)}{p_2 + O(\mathbf{x},t)}\right)\left(\frac{G(\mathbf{x},t)}{p_3 + G(\mathbf{x},t)}\right)\left(\frac{1}{H(\mathbf{x},t)}\right)^{n_g}\right], \tag{23}$$

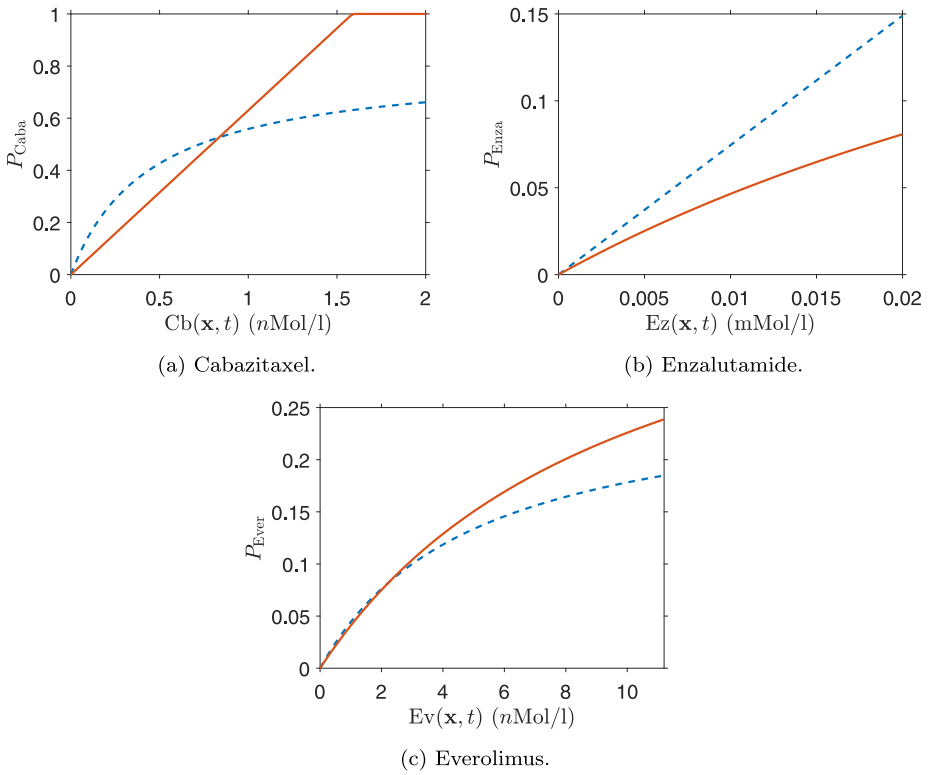

(a) Cabazitaxel. (b) Enzalutamide.

(c) Everolimus.

Fig. 3. Drug death probabilities, where the blue dotted line is S_p and the orange full line is R_p.

for $Y = R, S$. This is based on the proliferation function first introduced by Casciari et al. [39], where K_Y is the maximum proliferation rate for the specific phenotype, p_{1Y} is the fitness coefficient that determines how well cells are able to cope with a hostile environment, p_2 and p_3 are the half-maximum constants for the Michaelis–Menten kinetics for oxygen and glucose respectively, and $n_g < 1$ is a limiting factor on the impact of hydrogen.

Following the approach by Portz et al. [40], sensitive cells can proliferate in a symmetric ($S_p \mapsto S_p + S_p$) or asymmetric ($S_p \mapsto S_p + R_p$) way depending on a constant probability k_p, while resistant cells are assumed to proliferate symmetrically. After cell division, one of the daughter cells occupies one of the free neighbouring grid points, chosen at random, and the cell in the original grid point is checked to see if the enzalutamide concentration has caused it to change its resistance phenotype, while the new cell keeps the just assigned status until the end of its first life cycle. Based on experimental evidence [1], and as it can be observed in Fig. 4, the switch of S_p cells to resistant cells occurs with probability

$$P_{\text{Resis}} = \frac{\text{Ez}(\mathbf{x}, t)}{a_1 + \text{Ez}(\mathbf{x}, t)}, \tag{24}$$

and for R_p cells the switch to sensitive cells occurs with probability

$$P_{\text{Sensi}} = \frac{a_2}{a_2 + \text{Ez}(\mathbf{x}, t)}. \tag{25}$$

If a cell fails to proliferate, either due to no free neighbours or due to unfavourable conditions, the cell instead undergoes a phase switch and becomes quiescent.

2.3. Therapies

In the following section we show the simulations of different therapies that consider either a single drug or a pair, and with varying durations of treatment. All therapies assume that the drugs enter the tumour from the vasculature boundary region, and diffuse through the surrounding tissue without affecting the healthy cells. Since TRAMP

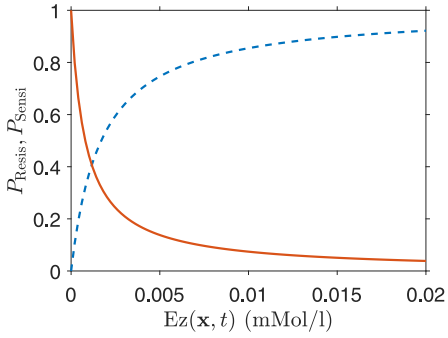

Fig. 4. Probability of differentiation from S_p to R_p (blue dotted line) and differentiation from R_p to S_p (orange full line).

mice start developing tumours around week seven or eight of their lives, and that by week 12 the tumours are visible, we assume for these simulations that they begin at week five of the TRAMP mice life cycle. In each therapy, the simulation is run for five weeks before the drugs are added in order to simulate the time required for the tumour to be discovered (i.e., in the experimental setting a lump becomes visible and/or can be felt by touch) and the treatments to begin.

As stated previously, we wish to consider the effectiveness of the drugs, both individually and with enzalutamide in combination with either cabazitaxel or everolimus. For the single-drug therapies, the drugs are administered over a 12, 18 and 52 week period. The combinations are administered over the same periods, but in two different ways which we refer to as "Then" therapy and "Alternating" therapy. For "Then" therapies enzalutamide is given by itself for the first half of the time period, with the other drug being administered over the second half. With "Alternating" therapies the drugs are administered alternately. For the cabazitaxel pair this means that enzalutamide is given for a week, and the next week cabazitaxel is given during the

middle of the week. For everolimus the drugs are administered on alternate days, starting with enzalutamide. This is done to avoid any toxic or pharmacokinetic interactions that could occur between the drugs [41]. Appendix B provides detailed illustrations of the treatment schedules for the various therapies.

3. Simulation process of the hybrid model

The model that we consider in this section is a multi-scale system with drug diffusion, where each time step of the simulation begins with solving the micro-environment PDEs. Because the disparity between the time scales of the micro-environment and the CA is very large, the changes in cells can be considered as adiabatic perturbations of the micro-environments. For this reason, following the ideas used by Patel et al. [42], the PDEs can be solved as elliptic boundary-value equations on a coarse time-scale rather than as parabolic diffusion equations explicit in time. This method does greatly increase the simulation efficiency, but can introduce discrepancies in the simulation as all cells react to changes in the micro-environment simultaneously. In order to avoid that, the CA is advanced in a series of random subsets of CA elements. This means that only a fraction, $f < 1$, of the CA elements is updated at a time, and after each fraction is updated the PDEs are solved again to determine the response of the micro-environment. This process is repeated until all of the CA elements have been updated, i.e. $1/f$ times. Patel et al. [42] found that there was no qualitative difference in the CA as long as $f < 0.2$. Therefore, for all simulations we considered $f = 0.1$. As the subsets are chosen randomly at each time step, this prevents all cells from being updated either simultaneously or in a spatially sequential manner. Given that, and that we have assumed that healthy prostate cells and necrotic cells do not consume or produce O, G and H, the micro-environment system (8) is different depending on the cell present at site $\mathbf{x}$. As such, the micro-environment system (8) for S_p, S_q, R_p and R_q becomes

$$D_c \nabla^2 c = g_c, \tag{26}$$

$$D_j \nabla^2 j = 0, \tag{27}$$

where $c = H, O, G, A$, $j = \text{Ez, Cb, Ev}$ and g_c are defined in (9). For healthy prostate and necrotic cells we take

$$D_k \nabla^2 k = 0, \tag{28}$$

where $k = H, O, G, \text{Ez, Cb, Ev}$.

To avoid conflicts in occupying space during proliferation, cells look at space availability with the current cell distribution as well as any sites that have already been updated by previous subsets. This allows space created by apoptosis or drug deaths to be used immediately, as well as preventing two cells proliferating into a shared neighbour.

To perform the numerical simulations we used MATLAB 2022a with the standard 5-point discretisation for the Laplacian operator.

4. Simulation results

The following simulations were carried out on a discretisation of the square region Ω by a 100×100 grid, in which each grid cell corresponds to an area $20\ \mu\text{m} \times 20\ \mu\text{m}$, chosen to be approximately the size of a single tumour cell [30]. We assumed that PCa cells cannot proliferate into the boundary region, and that oxygen, glucose and hydrogen have Dirichlet boundary conditions of 0.014 mMol/ℓ, 0.05 mMol/ℓ and 7.2 pH, respectively. The drug boundary conditions are as described above in Section 3 with the initial dose for each drug equal to $\text{Ez}^* = 0.02$ mMol/ℓ, $\text{Cb}^* = 1.79$ nMol/ℓ and $\text{Ev}^* = 11.2$ nMol/ℓ respectively. Initially a small cluster (3×3 grid sites) of S_p cells is placed in the centre of the grid, with the starting oxygen, glucose and hydrogen concentration being the respective initial condition throughout the domain. The simulation is then run for each therapy with one complete update cycle of the CA corresponding to one day (the parameter values taken for all simulations are given in Table A.1). For each 12 week therapy simulation the final cell distribution is illustrated, as well as the total populations of the sensitive and resistant phenotypes over time. For the 18 week therapies we show a comparison of the PCa cell coverage as a percentage of pathological area against data from Cerasuolo et al. [1]. We also consider the unrestricted growth of the tumour without treatment, to use it as a benchmark for comparison with the therapies.

As we have used stochastic elements throughout the CA, there is variation between multiple simulations of the same therapy, with each simulation having slight differences in tumour shape, coverage and cell phenotypes. The cell distribution figures that we present provide typical examples of those for the system undergoing each therapy. The main results presented in the paper are collected from 1500 simulation runs: 10 treatment types (9 summarised in detail in Appendix B, plus a no-treatment control) with 3 possible durations for each (12, Fig. B.1, 18, Fig. B.2, and 52 weeks, Fig. B.3), and 50 runs of each (with different random number seeds) to account for stochasticity in the random choices underlying the CA rules. The spatial distribution of cell types differs in individual runs. We therefore plot the extreme (minimum to maximum) values taken across all simulation runs against time, and also 95% confidence intervals for the population mean of the relevant quantities taken across all simulation runs against time. Doing this reveals that the qualitative behaviour and indeed the quantities of different cell types observed over time are both rather insensitive to such stochastic effects.

4.1. 12 week therapies

In Fig. 5, we can see the dynamics of untreated prostate cells in TRAMP mice, with a necrotic core forming at the centre of the tumour. The model's embedded stochasticity, which can be observed in the irregular shape of the tumour growth, is very clear after 84 and 126 days of tumour growth, but it can already be appreciated at week 11 of the TRAMP mice life cycle (35 days of the simulation).

Introducing enzalutamide causes the majority of the cell population to differentiate to the resistant phenotype, as seen in Fig. 6. We also note that oxygen concentration gradients determine preferential cellular proliferation paths, with tumour cells inhabiting the regions closest to the vasculature as they grow. After 12 weeks of therapy the tumour has yet to reach the corners of the grid. From week six it is possible to observe that small clusters of non-necrotic cells (between one and five cells together) form in the centre of the grid.

In contrast, cabazitaxel has a more pronounced effect on the distribution of the PCa cells, with it forming into a number of large clusters after 12 weeks of therapy, with a minimal presence on the edge of the vasculature, as seen in Fig. 7.

Fig. 8 shows the effect of everolimus on the tumour, with a final cell distribution similar to that of the enzalutamide therapy, though, as expected, little to no differentiation has occurred. We note that the PCa cells cover a larger region near the vasculature at 12 weeks than in Fig. 6(c), suggesting that everolimus is less effective at delaying the growth of the PCa tumour.

Comparing the single drug therapies, cabazitaxel-only seems to be the most effective over 12 weeks, resulting in a much curtailed cell distribution in comparison to the other two, as well as a lower total cell population. However, Fig. 9(b), (c) and (d) shows that for each therapy the total tumour cell population is steadily increasing, though at a much slower rate for cabazitaxel than the others, which suggests that these therapies will not be effective in the long run. Note also that for the enzalutamide-only therapy there is always a small population of sensitive cells that survives, Fig. 9(b). This is most likely caused by resistant cells switching to sensitive cells at a sufficient rate to replace those lost to drug death and apoptosis.

For the "Then" therapies we observe similar behaviour after six weeks of therapy as we do for the enzalutamide only therapy, as

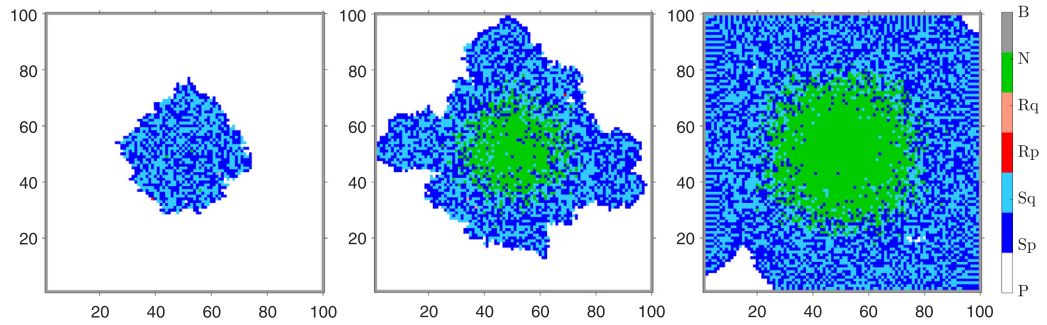

Fig. 5. Untreated PCa simulation over 119 days, at (a, left) 35 days, (b, middle) 77 days and (c, right) 119 days. The figure indicates the cell types: non-cancerous Prostate (P; white), Sensitive-proliferating (Sp; dark blue), Sensitive-quiescent (Sq; light blue), Resistant-proliferating (Rp; dark red), Resistant-quiescent (Rq; light red), Necrotic (N; green), and Boundary (B; grey).

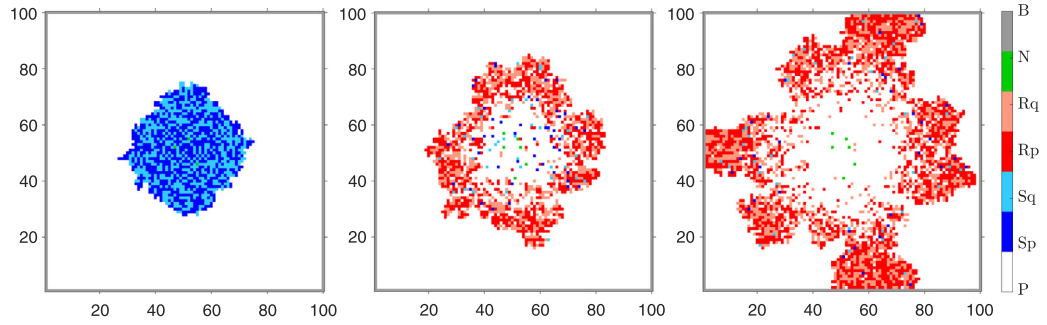

Fig. 6. Enzalutamide only, at (a, left) therapy start, (b, middle) 6 weeks of therapy and (c, right) 12 weeks of therapy.

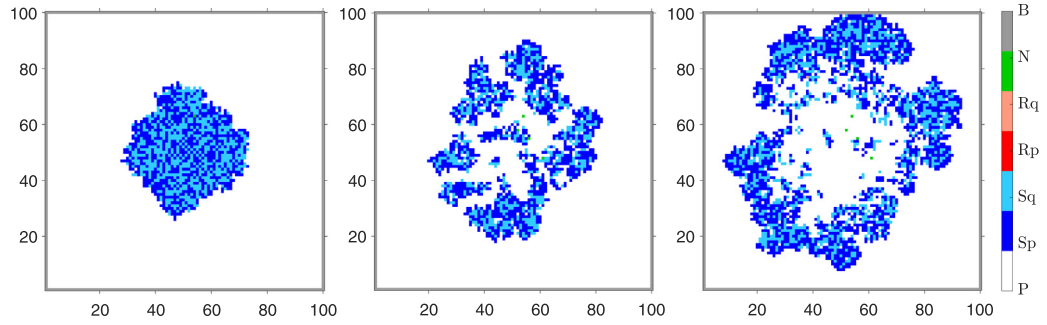

Fig. 7. Cabazitaxel only, at (a, left) therapy start, (b, middle) 6 weeks of therapy and (c, right) 12 weeks of therapy.

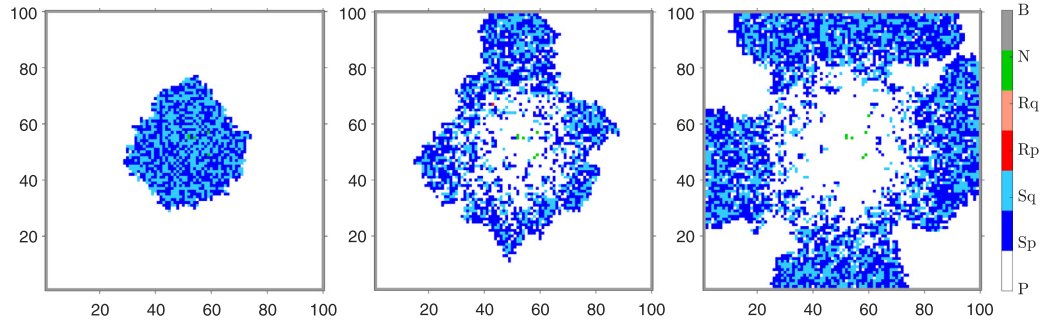

Fig. 8. Everolimus only, at (a, left) therapy start, (b, middle) 6 weeks of therapy and (c, right) 12 weeks of therapy.

expected, since for the first six weeks all of these therapies have enzalutamide only being given.

Fig. 10(c) shows that at the end of the "Then" cabazitaxel 12 week therapy the tumour cells are organised in a few large clusters, though

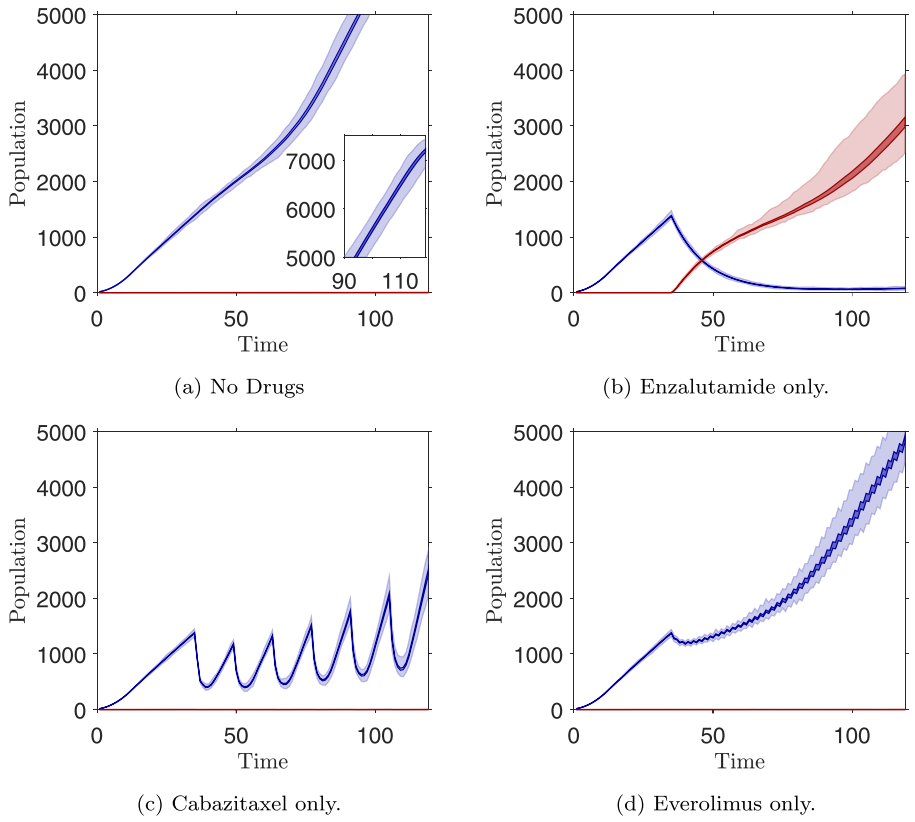

Fig. 9. The cell populations of the PCa phenotypes undergoing the single drug 12 week therapies. Blue indicates the sensitive phenotype and red indicates the resistant phenotype. The outer (transparent/light) regions indicate the extreme range of values taken (minimum to maximum) over an ensemble of $n = 50$ separate simulation runs of the model (with different random number seeds) for each treatment. The inner (solid/dark) regions indicate the 95% confidence intervals for the population mean across the runs (using the t-distribution with $n - 1$ degrees of freedom) against time. A common vertical axis, fitted to the worst of the treatments, is used to facilitate comparisons within this figure and with later figures. The inset in (a) shows the final (non-necrotic) cell population for the no-treatment control.

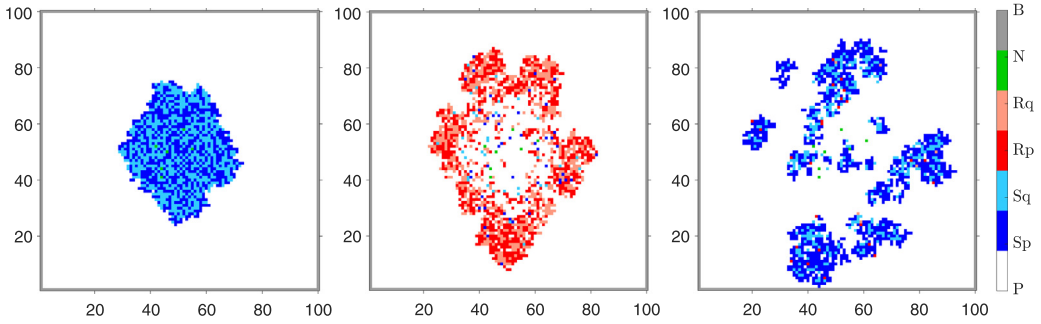

Fig. 10. "Then" cabazitaxel 12 week therapy, at (a, left) therapy start, (b, middle) 6 weeks of therapy and (c, right) 12 weeks of therapy.

with a greatly decreased population in comparison to the cabazitaxel (or enzalutamide) only therapy. We note that the sensitive phenotype is dominant in the cell population, which is to be expected in an enzalutamide-deficient environment and with the effectiveness of cabazitaxel at eliminating the resistant phenotype, as seen in Figs. 3(a) and 4 respectively.

In comparison, the "Then" everolimus 12 week therapy presents a cell distribution similar in shape, but smaller in size, to that of everolimus-only at 12 weeks, as seen in Fig. 11(c). The major difference is that there is a proportion of the cell population that is the resistant phenotype, which highlights the relative ineffectiveness of everolimus at eliminating the resistant cells.

While most of the therapies result in large regions of tumour cells, the "Alternating" cabazitaxel therapy results in very small clusters of tumour cells, as seen in Fig. 12(b) and (c). While this is a good indicator that this therapy could result in a tumour free state, these clusters could be small enough to be able to enter the vasculature by traversing capillary size vessels and become seeds for metastases, leading to serious complications [43,44].

The "Alternating" everolimus therapy is far more effective than the "Then" everolimus therapy, with the cell distribution heavily curtailed and the sensitive phenotype almost non-existent. As we can see in Fig. 13 the remaining cells are predominantly in around four or five large regions, with two reaching the vasculature, and a few small clusters close to these regions.

We note that all of the therapies stop the formation of a necrotic core, and that with all therapies the centre of the grid is mostly non-cancerous. As the boundary region represents the vasculature that

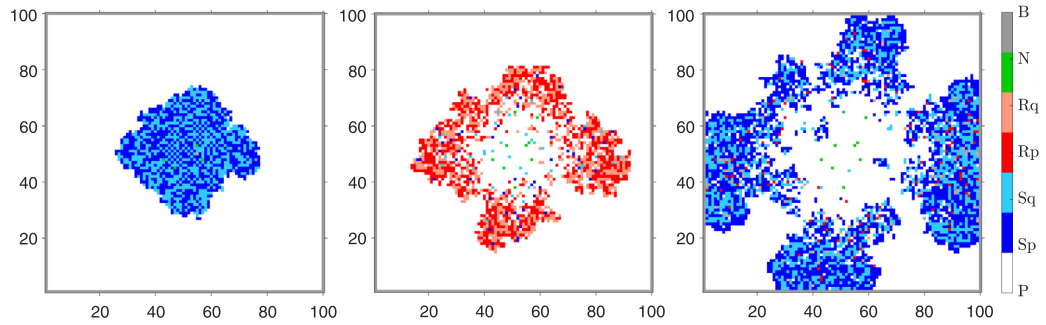

Fig. 11. "Then" everolimus 12 week therapy, at (a, left) therapy start, (b, middle) 6 weeks of therapy and (c, right) 12 weeks of therapy.

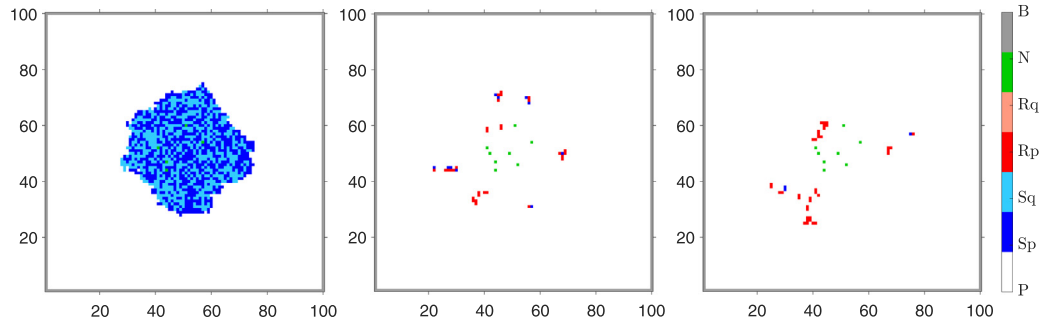

Fig. 12. "Alternating" cabazitaxel 12 week therapy, at (a, left) therapy start, (b, middle) 6 weeks of therapy and (c, right) 12 weeks of therapy.

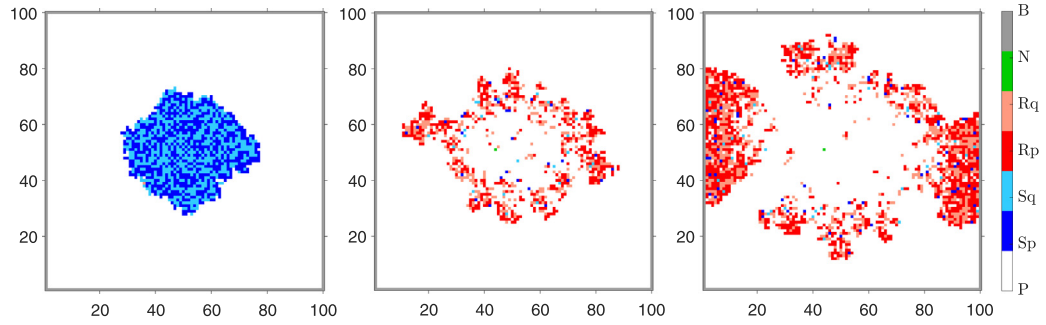

Fig. 13. "Alternating" everolimus 12 week therapy, at (a, left) therapy start, (b, middle) 6 weeks of therapy and (c, right) 12 weeks of therapy.

provides the nutrients to the region, it is unsurprising that the PCa cells survive and the tumour cell region migrates into the locations closest to it. While the drugs are also introduced from the boundaries, their micro-environment equations in (27) and (28) have harmonic solutions, making a cell's distance from the boundary not a factor in their survival from drug death.

We observe that "Alternating" therapies and the "Then" cabazitaxel therapy are more effective than the single drug therapies (Fig. 9) at reducing the total cell population (Fig. 14). While the cabazitaxel combination therapies have a lower final cell population than the "Then" everolimus therapy, the cell population oscillates around the doses, while the "Then" everolimus therapy is more uniform.

4.2. 18 Week therapies

No significant difference is observed in the untreated tumour after a further six weeks of cell growth. Untreated PCa cells still develop a necrotic core, while all of the therapies prevent the necrotic core from forming. Increasing the duration of the single drug therapies causes the cell populations to plateau for enzalutamide and everolimus, suggesting that the effectiveness of the drugs at stopping the tumour growth is limited, and that the micro-environment conditions become the limiting factor.

We note that the "Then" everolimus therapy has a much reduced resistant cell population, and that the cell distribution is similar to that of the everolimus-only therapy, Fig. 15(b) and (a) respectively. This suggests that the effectiveness of the "Then" everolimus therapy is more limited the longer it is used.

From Fig. 15(c) we see that the "Alternating" cabazitaxel therapy still has clusters of PCa cells after the additional six weeks of therapy. This suggests that the risk of metastases is present for both the 12 and 18 week therapies.

The other combination therapies are more effective than the single drug therapies, but "Then" cabazitaxel and "Alternating" everolimus both indicate an increase in tumour cell population over the respective 12 week therapies, though not as pronounced as the single drug therapies (not shown).

To determine the accuracy of our simulations, the PCa cell coverage was computed over the 18 week therapies and compared against the data from TRAMP mice in [1]. As we see in Fig. 16, our simulations fall within the natural variation observed in living organisms. These graphs allow us to be confident that our simulations are reasonable

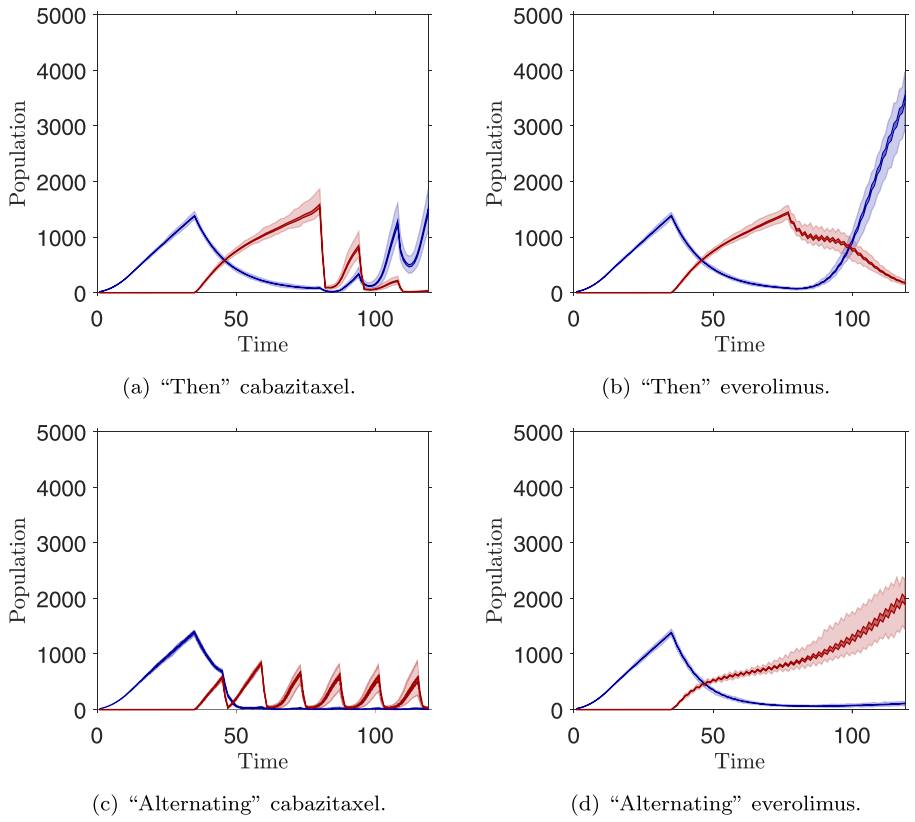

(a) "Then" cabazitaxel. (b) "Then" everolimus.

(c) "Alternating" cabazitaxel. (d) "Alternating" everolimus.

Fig. 14. The cell populations of the PCa phenotypes undergoing the 12 week therapies. Blue indicates the sensitive phenotype and red indicates the resistant phenotype. The outer (transparent/light) regions indicate the range of values taken (minimum to maximum) over an ensemble of $n = 50$ separate simulation runs of the model for each treatment. The inner (solid/dark) regions indicate the 95% confidence intervals for the population mean across the runs, plotted against time. A common vertical axis is used to facilitate comparisons.

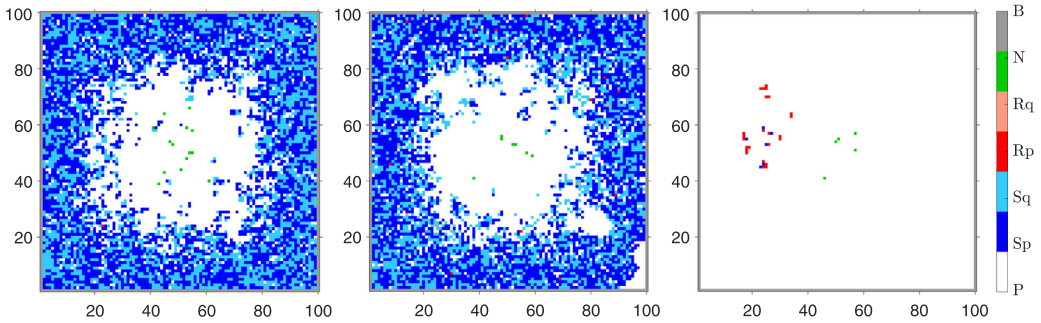

Fig. 15. Final cell distributions after 18 weeks of therapy: (a, left) Everolimus only, (b, middle) "Then" everolimus, (c, right) "Alternating" cabazitaxel.

approximations of the tumour's behaviour, and as such the therapies we considered can provide reasonable predictions of the tumour behaviour in the short and long term.

4.3. Year long therapies

For the year long therapies we note that although the "Alternating" cabazitaxel therapy appears capable of achieving a tumour-free state, with the parameter values used in the model it leads to a suppressed but persistent tumour population with sustained oscillations. For example, the picture shown in Fig. 17(c), at the end of the final week of treatment, might appear to suggest that the tumour-free state will be reached with a short course of further treatment. However, Fig. 17(d) from the start of the same week reveals the presence of clusters of PCa cells that continue to oscillate in size as shown in Fig. 17(e). Simulations of an "enzalutamide with cabazitaxel" therapy (which is used to calibrate the model) B.3(h), in which the boundary value concentration of enzalutamide is kept constant throughout treatment, does reach a tumour-free state, although stochastic effects lead to a large variance in the time taken to reach the tumour-free state for different runs and the treatment is unlikely to be suitable for clinical use. Increasing the maximum boundary value concentration of cabazitaxel to $\mathrm{Cb}^* = 1.85$ nMol/ℓ during the "alternating" therapy appears to cause a bifurcation in the dynamics, typically resulting in a tumour-free state before the end of the year-long therapy: Fig. 17(f) shows 95% confidence intervals for the mean tumour population across 50 simulation runs, 48% of which achieved a tumour-free state by week 26 of treatment, 80% by week 39, and 96% by week 52.

The other therapies do not produce such a result, with all of them either maintaining the conditions reached already with the 18 week

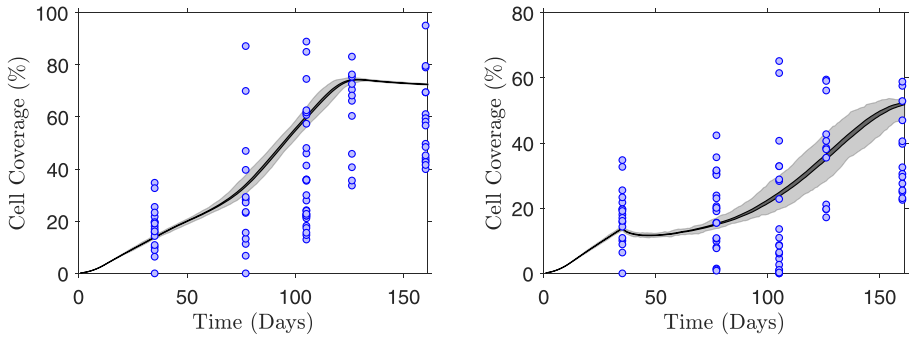

(a) Cell coverage percentage for untreated PCa simulation.

(b) Cell coverage percentage for enzalutamide only therapy.

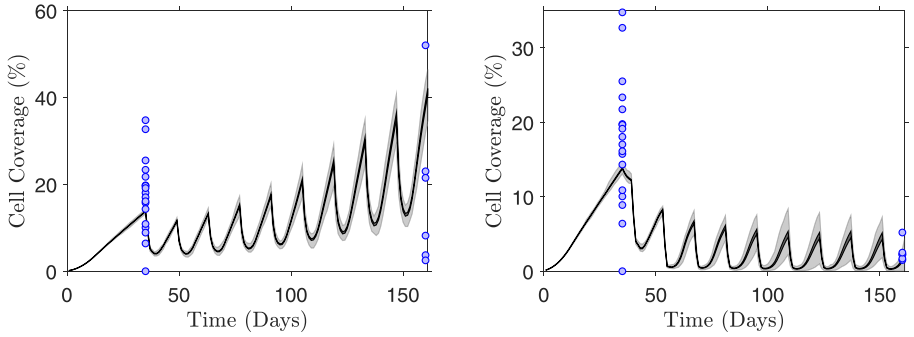

(c) Cell coverage percentage for cabazitaxel only therapy.

(d) Cell coverage percentage for "Alternating" cabazitaxel therapy.

Fig. 16. Cell coverage percentage for different therapies against data (blue dots) from [1]. In each graph the circles are the data points, the outer (grey) region shows the extreme range of values taken (minimum to maximum) across 50 simulation runs against time, and the inner solid (black) regions show the 95% confidence interval for the population mean value computed across the runs plotted against time.

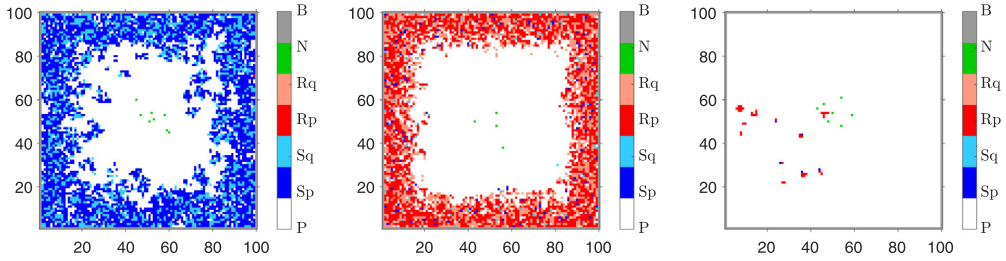

(a) "Then" cabazitaxel.

(b) "Alternating" everolimus.

(c) "Alternating" cabazitaxel.

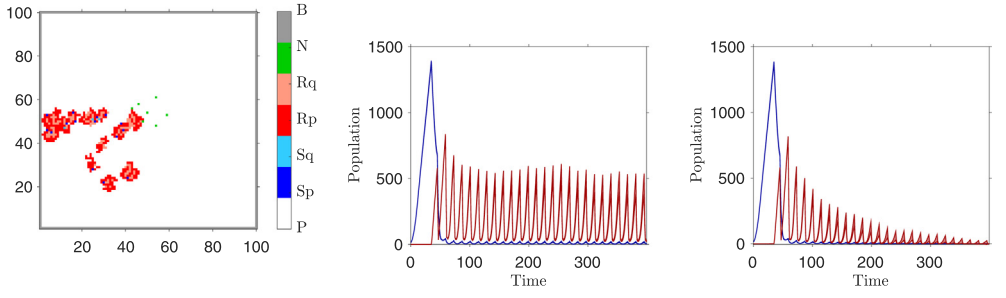

(d) "Alternating" cabazitaxel.

(e) "Alternating" cabazitaxel.

(f) "Alternating" cabazitaxel.

Fig. 17. Final cell distributions after year long therapy for (a) "Then" cabazitaxel, (b) "Alternating" everolimus, and (c) "Alternating" cabazitaxel for which (d) shows the cell distribution at the start of the final week of therapy and (e,f) show 95% confidence intervals for the mean of the tumour population over 50 simulation runs against time with blue indicating the sensitive phenotype and red the resistant phenotype, with (f) showing the success of a higher-dosage version of the therapy in driving the mean towards zero over the space of the 52 week therapy. For (f), 48% of the runs achieved a tumour-free state by week 26 of treatment, 80% by week 39, and 96% by week 52.

Table A.1
Parameters for the simulations of the model, where references marked by ∗ are model specific parameters and units marked by — indicate dimensionless quantities.

Param	Definition	Value	Units	Ref
δ_{Cb}	Cabazitaxel maximum mortality probability for sensitive cells	0.81	–	[1]
δ_{Ev}	Everolimus maximum mortality probability for sensitive cells	0.268	–	[1]
δ_{Ez}	Enzalutamide efficacy on sensitive cells	7.45	ℓ/mMol	[1]
η_{Cb}	Cabazitaxel degradation rate	0.25	1/day	[1]
η_{Ev}	Everolimus degradation rate	0.8	1/day	[1]
η_{Ez}	Enzalutamide degradation rate	0.17	1/day	[1]
λ_{Cb}	Cabazitaxel efficacy on resistant cells	0.63	ℓ/nMol	[1]
λ_{Ev}	Everolimus maximum mortality probability for resistant cells	0.454	–	[1]
λ_{Ez}	Enzalutamide maximum mortality probability for resistant cells	0.308	–	[1]
a_1	Half saturation level for sensitive to resistant switching	0.0017	mMol/ℓ	[1]
a_2	Half Saturation level for resistant to sensitive switching	0.0008	mMol/ℓ	[1]
ATP_d	ATP threshold for apoptosis	0.3	mMol/ℓ	[30]
ATP_q	ATP threshold for quiescence	0.8	mMol/ℓ	[30]
D_{Cb}	Cabazitaxel diffusion rate	800	$\mu m^2/s$	[45]
D_{Ev}	Everolimus diffusion rate	800	$\mu m^2/s$	[45]
D_{Ez}	Enzalutamide diffusion rate	800	$\mu m^2/s$	[45]
D_G	Glucose diffusion rate	500	$\mu m^2/s$	[30]
D_H	Hydrogen ion diffusion rate	1080	$\mu m^2/s$	[30]
D_O	Oxygen diffusion rate	1820	$\mu m^2/s$	[30]
k_a	Apoptosis stiffness coefficient	0.1×10^3	ℓ/mMol	∗
k_{Cb}	Cabazitaxel half-maximum mortality coefficient for sensitive cells	0.45	nMol/ℓ	[1]
k_{EvR}	Everolimus half-maximum mortality coefficient for resistant cells	10.1	nMol/ℓ	[1]
k_{EvS}	Everolimus half-maximum mortality coefficient for sensitive cells	5.04	nMol/ℓ	[1]
k_{Ez}	Enzalutamide half-maximum mortality coefficient for resistant cells	0.0563	mMol/ℓ	[1]
k_G	Half-Maximum glucose concentration for consumption	0.04	mMol/ℓ	[30]
k_H	Half-maximum hydrogen ion concentration	2.5×10^{-4}	–	[30]
k_N	Necrotic stiffness coefficient	2.5×10^3	ℓ/mMol	∗
k_O	Half-maximum oxygen concentration for consumption	0.005	mMol/ℓ	[30]
k_p	Probability of random mutation	0.0002	–	[10]
K_R	Maximum proliferation rate for resistant cells	0.907	1/day	[1]
K_S	Maximum proliferation rate for sensitive cells	1.15	1/day	[1]
k_q	Quiescence stiffness coefficient	0.07×10^3	ℓ/mMol	∗
n_g	Limiting factor on the impact of hydrogen	0.4566	–	[39]
O_N	Necrotic threshold	0.002	mMol/ℓ	∗
p_{1R}	Fitness coefficient for resistant cells	0.02	–	[1]
p_{1S}	Fitness coefficient for sensitive cells	0.0146	–	[1]
p_2	Half maximum oxygen coefficient for proliferation	7.29×10^{-3}	mMol/ℓ	[39]
p_3	Half maximum glucose coefficient for proliferation	1.76×10^{-2}	mMol/ℓ	[39]
p_{g_R}	Glucose metabolism multiplier for resistant cells	4	–	[1]
p_{g_S}	Glucose metabolism multiplier for sensitive cells	1.3	–	[1]
V_{OR}	Maximum oxygen consumption for resistant cells	0.0216	mMol/ℓ/s	[1]
V_{OS}	Maximum oxygen consumption for sensitive cells	0.0288	mMol/ℓ/s	[1]

therapies, or resulting in worse conditions in the case of the "Then" cabazitaxel and "Alternating" everolimus therapies, Figs. 17(a) and 17(b) respectively.

5. Discussion

In this paper we proposed a novel hybrid CA to simulate and investigate the effectiveness of various chemotherapy drugs on PCa. We assumed that the differentiation of the PCa cells was motivated by the concentration of the first chemotherapy drug we considered, enzalutamide, and by random mutation. This differentiation would be to a phenotype resistant to enzalutamide, but that was more vulnerable to other chemotherapy drugs [1]. Another key factor in our model was the use of particular probability functions in the CA rules, which helped to convey some of the differences seen between individual tumours [26]. Through numerical simulations we showed some of the possible prognoses resulting from the therapies, having considered single drug use, alternating doses of pairs of drugs and enzalutamide-only followed by another drug for a given period. These simulations also considered several different time frames, so that we could assess the effectiveness of both short-term and long-term treatment plans following particular patterns.

From the short term simulations (12 to 18 week therapies) we can see that cabazitaxel is the most effective of the single drug therapies, resulting in a lower total tumour cell population, even though it oscillates with the two weeks between doses. Both enzalutamide and everolimus result in larger cell populations, but the population is less volatile. Most of the combination therapies are more effective than the single drug therapies, with only "Then" everolimus 18 week therapy (Fig. 15(b)) having a larger PCa tumour cell population than the cabazitaxel only therapy, while the "Alternating" cabazitaxel 18 week therapy results in a steadily decreasing PCa cell population that leads almost to extinction in the simulation as shown in Fig. 15(c).

The year long therapies show, for most of our considered therapies, that long-term use is actually less effective than the results of short-term use might suggest, and either the treatment maintains the condition shown under the 18 week therapy, or the PCa cells continue to grow. The only exception is the "Alternating" cabazitaxel therapy, which consistently leads to a tumour-free state before the end of the year long therapy if given at a slightly higher dosage (Fig. 17(f)), but otherwise tends to result in sustained small oscillations (Fig. 17(e)). While these results are encouraging, the cell distributions of the "Alternating" cabazitaxel 12 week and 18 week therapies (Figs. 12 and 15(c) respectively) show very small clusters of PCa cells. These clusters are small enough to allow metastases to occur [44]. Therefore while this therapy is encouraging in the long term, care must be taken that short term issues do not arise. As each treatment has different quality-of-life concerns for the patients, we conclude that the enzalutamide-cabazitaxel alternating therapy could be used as a long term strategy for combating PCa, but that further research and clinical studies must be considered to counter possible metastases.

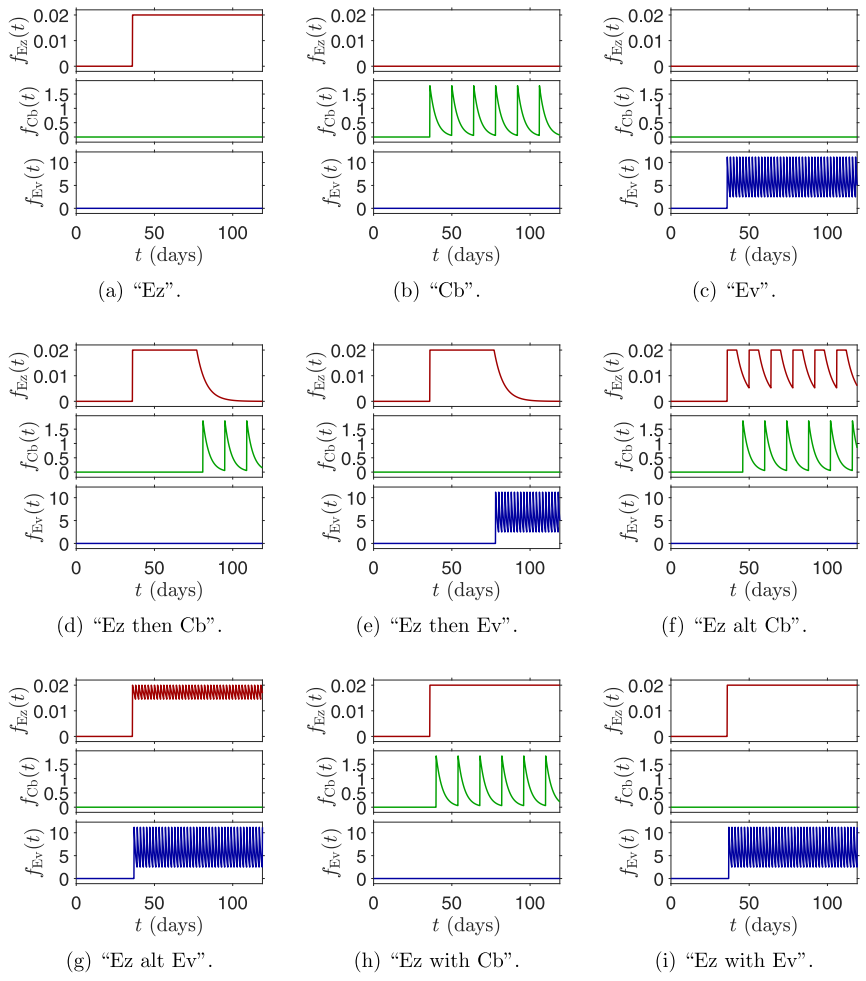

Fig. B.1. Drug treatment schedules for 12-week therapies, each showing the boundary conditions $f_{Ez}(t)$ (top; red in colour copy), $f_{Cb}(t)$ (middle; green in colour copy), and $f_{Ev}(t)$ (bottom; blue in colour copy): (a) Enzalutamide only, (b) Cabazitaxel only, (c) Everolimus only, (d) Enzalutamide then Cabazitaxel, (e) Enzalutamide then Everolimus, (f) Enzalutamide alternating Cabazitaxel, (g) Enzalutamide alternating Everolimus, (h) Enzalutamide with Cabazitaxel, (i) Enzalutamide with Everolimus.

We were able to compare the 18 week therapy simulations against the TRAMP mice data from [1], which allowed us to consider the accuracy of our simulations, all of which were well within the natural variations expected *in vivo*. We believe this means that our simulations are a good approximation for the PCa behaviour.

The model provides several avenues for further study. We have assumed that the healthy prostate cells have minimal impact on the micro-environment equations, and are not affected by the chemotherapy drugs introduced. Introducing CA rules that would govern how the healthy prostate cells behave as well as considering their interactions with the micro-environment could allow for greater accuracy in the model [21,46]. Another assumption in the model is that the vasculature is only present as a boundary region; it could instead be randomly scattered throughout the grid with a suitable distribution chosen to better represent the capillary network and periodic boundary conditions. Alternatively image analysis could be used to help develop mathematical models of tumour vasculature and angiogenesis [47]. This would provide a more faithful representation of prostate tissue composition, and could also lead to incorporating angiogenesis, in addition to allowing larger grids to be investigated and mitigating geometrical effects [21,31,48].

While we have considered three drugs in this model, there are many more that are used in ongoing clinical trials, and the model could be expanded to include them, especially those that are already being used in combination with the three considered in our study, such as docetaxel and abiraterone, and optimal control techniques could be used to design the best therapeutic strategy to eliminate the tumour from the organism [41,49]. We could also consider other combination therapies, such as all three drugs provided alternately, or cabazitaxel or everolimus first, then enzalutamide. However, one should note that drugs and drug combinations need to be carefully analysed in terms of their toxicity towards healthy cells, and that care is taken to ensure that no harm is done to the test subject. Alternative delivery mechanisms, such as direct injection to the tissue rather than diffusion from the vasculature, could also be considered. Also, as further clinical trials are performed, the pharmacokinetic pathways of these drugs are better understood, and the possible drug–drug interactions are discovered, the equations that govern the pharmacokinetic and the probability functions that govern drug death should be updated and improved to better replicate the real cellular behaviour [50,51]. Regarding the pharmacokinetic, another limitation of the model is related to the assumption that an adaptive therapy takes place, which disregards the possibility of drug accumulation. While adaptive therapies are possible and have attracted the attention of researchers in recent

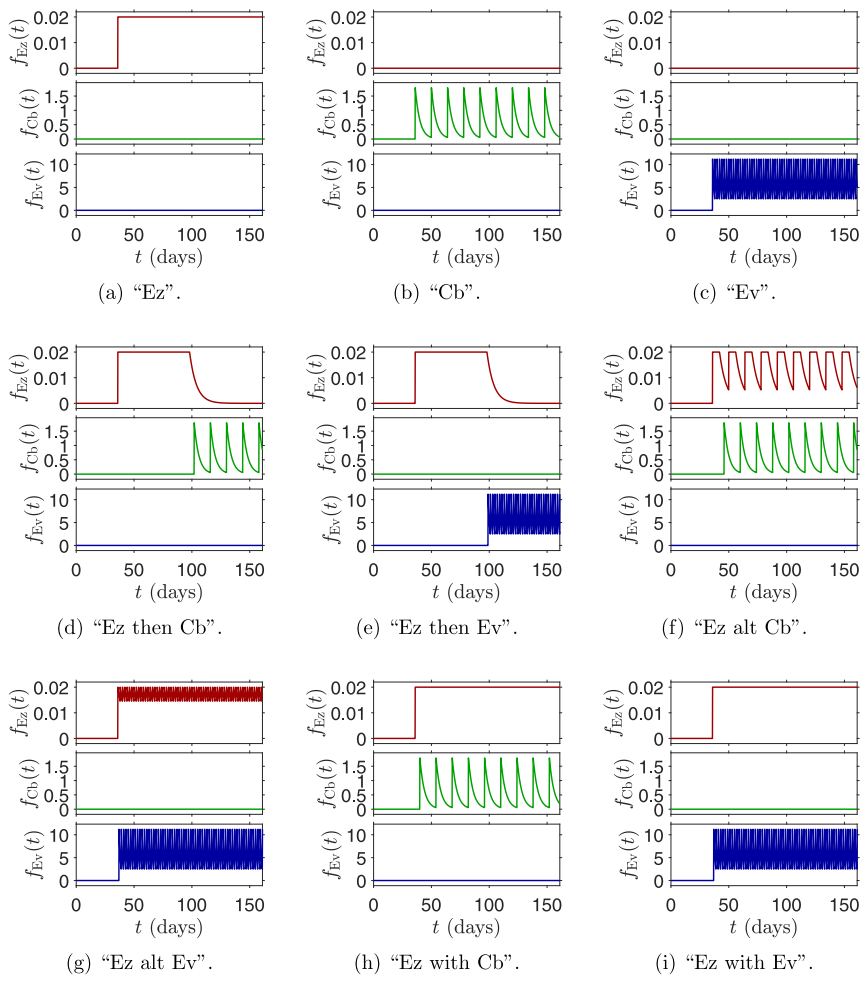

Fig. B.2. Drug treatment schedules for 18-week therapies, each showing the boundary conditions $f_{Ez}(t)$ (top; red in colour copy), $f_{Cb}(t)$ (middle; green in colour copy), and $f_{Ev}(t)$ (bottom; blue in colour copy): (a) Enzalutamide only, (b) Cabazitaxel only, (c) Everolimus only, (d) Enzalutamide then Cabazitaxel, (e) Enzalutamide then Everolimus, (f) Enzalutamide alternating Cabazitaxel, (g) Enzalutamide alternating Everolimus, (h) Enzalutamide with Cabazitaxel, (i) Enzalutamide with Everolimus.

years [52], they are not the most usual form of treatments as in the majority of cases patients are repeatedly injected with fixed-dose injections that lead to an accumulation of drugs in the blood flow and do not allow to maintain a target drug concentration as considered in the model. Finally, we would like to observe that the model is based on experiments on mice and is highly simplified overall; further work will be needed to obtain a mathematical modelling framework able to support research in humans and clinical trials. First of all, we would like to underline that the choice of a 2D approximation (tumour slice) could be extended by considering 3D tissue volumes with a more realistic vasculature geometry [19,53]. Secondly, since future models should extend to human tumours, this raises the issue of model parameterisation. Given the high number of parameters, we believe that the first step will be to select, through mathematical techniques such as sensitivity analysis [54], those few parameters that play a major role in the tumour growth and focus our attention on patient-specific simulations and therapies [55].

Declaration of competing interest

The authors declare that they have no known competing financial interests or personal relationships that could have appeared to influence the work reported in this paper.

Data availability

The code used to produce the simulations in this paper is available freely from the Zenodo repository [56].

Acknowledgements

The authors thank Dr C. Dunlop and Dr. J. Foster for helpful discussions. The authors would also like to thank the referees for their careful reading of the draft manuscript and their insightful comments that helped to improve the paper significantly.

Appendix A. Model parameters

See Table A.1.

Appendix B. Treatment schedules

Figs. B.1–B.3 demonstrate the drug schedules (showing the boundary conditions) for various 12, 18, and 52-week therapies, respectively. Therapies (h,i) are used to help calibrate the model.

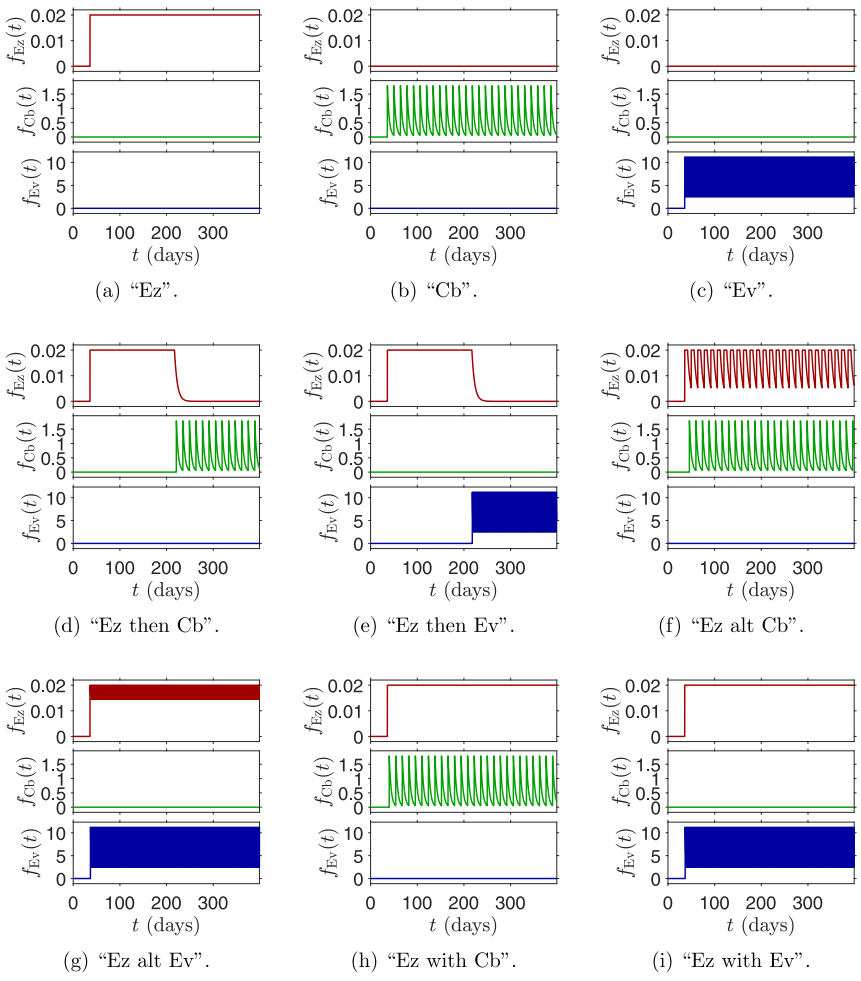

Fig. B.3. Drug treatment schedules for 52-week therapies, each showing the boundary conditions $f_{Ez}(t)$ (top; red in colour copy), $f_{Cb}(t)$ (middle; green in colour copy), and $f_{Ev}(t)$ (bottom; blue in colour copy): (a) Enzalutamide only, (b) Cabazitaxel only, (c) Everolimus only, (d) Enzalutamide then Cabazitaxel, (e) Enzalutamide then Everolimus, (f) Enzalutamide alternating Cabazitaxel, (g) Enzalutamide alternating Everolimus, (h) Enzalutamide with Cabazitaxel, (i) Enzalutamide with Everolimus.

References

[1] M. Cerasuolo, F. Maccarinelli, D. Coltrini, A. Mahmoud, V. Marolda, G. Ghedini, S. Rezzola, A. Giacomini, L. Triggiani, M. Kostrzewa, R. Verde, D. Paris, D. Melck, M. Presta, A. Ligresti, R. Ronca, Modeling acquired resistance to the second-generation androgen receptor antagonist enzalutamide in the tramp model of prostate cancer, Cancer Res. 80 (7) (2020) 1564–1577, http://dx.doi.org/10.1158/0008-5472.CAN-18-3637.

[2] F. Bray, J. Ren, E. Masuyer, J. Ferlay, Global estimates of cancer prevalence for 27 sites in the adult population in 2008, Int. J. Cancer 132 (5) (2012) 1133–1145, http://dx.doi.org/10.1002/ijc.27711.

[3] W.H. Organisation, https://gco.iarc.fr/today, last Accessed: 2020-06-05.

[4] Prostate cancer statistics, 2019, https://www.cancerresearchuk.org/health-professional/cancer-statistics/statistics-by-cancer-type/prostate-cancer#heading-Zero, last Accessed: 2019-09-01.

[5] About prostate cancer, 2019, https://prostatecanceruk.org/prostate-information/about-prostate-cancer, last Accessed: 2019-09-01.

[6] T. Jackson, A mathematical model of prostate tumor growth and androgen-independent relapse, Discrete Contin. Dyn. Syst. Ser. B 4 (2004) 187–201, http://dx.doi.org/10.3934/dcdsb.2004.4.187.

[7] N. Mottet, R.C. van den Bergh, E. Briers, T. Van den Broeck, M.G. Cumberbatch, M. De Santis, S. Fanti, N. Fossati, G. Gandaglia, S. Gillessen, N. Grivas, J. Grummet, A.M. Henry, T.H. van der Kwast, T.B. Lam, M. Lardas, M. Liew, M.D. Mason, L. Moris, D.E. Oprea-Lager, H.G. van der Poel, O. Rouvière, I.G. Schoots, D. Tilki, T. Wiegel, P.-P.M. Willemse, P. Cornford, Eau-eanm-estro-esur-siog guidelines on prostate cancer—2020 update. Part 1: Screening, diagnosis, and local treatment with curative intent, Eur. Urol. 79 (2) (2021) 243–262, http://dx.doi.org/10.1016/j.eururo.2020.09.042.

[8] P. Cornford, R.C. van den Bergh, E. Briers, T. Van den Broeck, M.G. Cumberbatch, M. De Santis, S. Fanti, N. Fossati, G. Gandaglia, S. Gillessen, N. Grivas, J. Grummet, A.M. Henry, T.H. van der Kwast, T.B. Lam, M. Lardas, M. Liew, M.D. Mason, L. Moris, D.E. Oprea-Lager, H.G. van der Poel, O. Rouvière, I.G. Schoots, D. Tilki, T. Wiegel, P.-P.M. Willemse, N. Mottet, Eau-eanm-estro-esur-siog guidelines on prostate cancer. Part ii—2020 update: Treatment of relapsing and metastatic prostate cancer, Eur. Urol. 79 (2) (2021) 263–282, http://dx.doi.org/10.1016/j.eururo.2020.09.046.

[9] H. Miyamoto, E. Messing, C. Chang, Does androgen deprivation improve treatment outcomes in patients with low-risk and intermediate-risk prostate cancer? Nat. Rev. Clin. Oncol. 2 (2005) 236–237, http://dx.doi.org/10.1038/ncponc0168.

[10] M. Cerasuolo, D. Paris, F.A. Iannotti, D. Melck, R. Verde, E. Mazzarella, A. Motta, A. Ligresti, Neuroendocrine transdifferentiation in human prostate cancer cells: an integrated approach, Cancer Res. 75 (15) (2015) 2975–2986, http://dx.doi.org/10.1158/0008-5472.CAN-14-3830.

[11] H. Beltran, T. Beer, M. Carducci, J. de Bono, M. Gleave, H.M.W. Kelly, F. Saad, C. Sternberg, S. Tagawa, I. Tannock, New therapies for castration-resistant prostate cancer:efficacy and safety, Eur. Urol. 60 (2) (2011) 279–290, http://dx.doi.org/10.1016/j.eururo.2011.04.038.

[12] Prostate cancer treatment, 2021, https://www.nhs.uk/conditions/prostate-cancer/treatment/#::text=Radiotherapy%20involves%20using%20radiation%20to,that's%20spread%20and%20relieve%20symptoms, last Accessed: 2021-04-01.

[13] R. Padmanabhan, N. Meskin, A.-E. Al Moustafa, Mathematical Models of Cancer and Different Therapies, Springer, 2021, http://dx.doi.org/10.1007/978-981-15-8640-8.

[14] A.R. Anderson, V. Quaranta, Integrative mathematical oncology, Nat. Rev. Cancer 8 (3) (2008) 227–234, http://dx.doi.org/10.1038/nrc2329.

[15] Y. Tang, L. Wang, O. Goloubeva, M. Khan, B. Zhang, A. Hussain, Divergent effects of castration on prostate cancer in tramp mice: possible implications for therapy, Clin. Cancer Res. 14 (10) (2008) 2936–2943, http://dx.doi.org/10.1158/1078-0432.CCR-07-4925.

[16] A. Retter, F. Gong, T. Syer, S. Singh, S. Adeleke, S. Punwani, Emerging methods for prostate cancer imaging: evaluating cancer structure and metabolic alterations more clearly, Mol. Oncol. 15 (10) (2021) 2565–2579, http://dx.doi.org/10.1002/1878-0261.13071, arXiv:https://febs.onlinelibrary.wiley.com/doi/pdf/10.1002/1878-0261.13071.

[17] H. Greenspan, Models for the growth of a solid tumour by diffusion, Int. J. Rad. Oncol. 51 (1972) 317–340, http://dx.doi.org/10.1002/sapm1972514317.

[18] J. Sherratt, M. Chaplain, A new mathematical model for avascular tumour growth, J. Math. Biol. 43 (2001) 291–312, http://dx.doi.org/10.1007/s002850100088.

[19] D. Hormuth II, J. Weis, S. Barnes, M. Miga, E. Rericha, V. Quaranta, T. Yankeelov, A mechanically coupled reaction–diffusion model that incorporates intra-tumoural heterogeneity to predict *in vivo* glioma growth, J. R. Soc. Interface 14 (2017) 20161010, http://dx.doi.org/10.1098/rsif.2016.1010.

[20] T. Quinn, Z. Sinkala, Dynamics of prostate cancer stem cells with diffusion and organism response, BioSystems 96 (2009) 69–79, http://dx.doi.org/10.1016/j.biosystems.2008.11.010.

[21] A. Anderson, M. Chaplain, Continuous and discrete mathematical models of tumor-induced angiogenesis, Bull. Math. Biol. 60 (1998) 857–900, http://dx.doi.org/10.1006/bulm.1998.0042.

[22] T. Alarcon, H. Byrne, P. Maini, A multiple scale model for tumor growth, Multiscale Model. Simul. 3 (2) (2005) 440–475, http://dx.doi.org/10.1137/040603760.

[23] H.M. Byrne, I.v. Leeuwen, M.R. Owen, T. Alarcón, P.K. Maini, Multiscale Modelling of Solid Tumour Growth, Birkhäuser Boston, Boston, 2008, pp. 1–25, http://dx.doi.org/10.1007/978-0-8176-4713-1-17.

[24] J. Osborne, A. Walter, S. Kershaw, G. Mirams, A. Fletcher, P. Pathmanathan, D. Gavaghan, O. Jensen, P. Maini, H. Byrne, A hybrid approach to multi-scale modelling of cancer, Phil. Trans. R. Soc. A 368 (2010) 5013–5028, http://dx.doi.org/10.1098/rsta.2010.0173.

[25] A. Almet, P. Maini, D. Moulton, H. Byrne, Modeling perspectives on the intestinal crypt, a canonical system for growth, mechanics, and remodeling, Curr. Opin. Biomd. Eng. 15 (2020) 32–39, http://dx.doi.org/10.1016/j.cobme.2019.12.012.

[26] A. Lopez, J. Seoane, M. Sanjuan, Dynamics of the cell-mediated immune response to tumour growth, Phil. Trans. R. Soc. A 375 (2017) 20160291, http://dx.doi.org/10.1098/rsta.2016.0291.

[27] C. Sosa-Marrero, R. De Crevoisier, A. Hernandez, P. Fontaine, N. Rioux-Leclerq, R. Mathieu, A. Fautrel, F. Paris, O. Acosta, Towards a reduced *in silico* model predicting biochemical recurrence after radiotherapy in prostate cancer, IEEE Trans. Biomed. Eng. (2021) 1, http://dx.doi.org/10.1109/TBME.2021.3052345.

[28] L. Turner, A. Burbanks, M. Cerasuolo, Mathematical insights into neuroendocrine transdifferentiation of numan prostate cancer cells, Nonlinear Anal. Model. Control 26 (5) (2021) 884–913, http://dx.doi.org/10.15388/namc.2021.26.24441.

[29] L. Turner, A. Burbanks, M. Cerasuolo, Pca dynamics with neuroendocrine differentiation and distributed delay, Math. Biosci. Eng. 18 (6) (2021) 8577–8602, http://dx.doi.org/10.3934/mbe.2021425.

[30] M. Robertson-Tessi, R.J. Gillies, R.A. Gatenby, A.R. Anderson, Impact of metabolic heterogeneity on tumor growth, invasion, and treatment outcomes, Cancer Res. 75 (8) (2015) 1567–1579, http://dx.doi.org/10.1158/0008-5472.CAN-14-1428.

[31] A. Ibrahim-Hashim, M. Robertson-Tessi, P. Enriquez-Navas, M. Damaghi, Y. Balagurunathan, J. Wojtkowiak, S. Russell, K. Yoonseok, M. Lloyd, M. Bui, J. Brown, A. Anderson, R. Gillies, R. Gatenby, Defining cancer subpopulations by adaptive stratgies rather than molecular properties provides novel insights into intratumoral evolution, Cancer Res. 77 (9) (2017) 2242–2254, http://dx.doi.org/10.1158/0008-5472.CAN-16-2844.

[32] G. Cicero, R. de Luca, P. Dorangricchia, F. Dieli, The clinical efficacy of enzalutamide in metastatic prostate cancer: prospective single-center study, Anticancer Res. 37 (3) (2017) 1475–1480, http://dx.doi.org/10.21873/anticanres.11472.

[33] F. Claessens, C. Helsen, S. Prekovic, et al., Emerging mechanisms of enzalutamide resistance in prostate cancer, Nat. Rev. Urol. 11 (2014) 712–720, http://dx.doi.org/10.1038/nrurol.2014.243.

[34] M. Jordan, L. Wilson, Microtubules as a target for anticancer drugs, Nat. Rev. Cancer 4 (4) (2004) 253–265, http://dx.doi.org/10.1038/nrc1317.

[35] C. Paller, E. Antonarakis, Cabazitaxel: a novel second-line treatment for metastatic castration-resistant prostate cancer, Drug Des. Dev. Therapy 5 (2011) 117–124, http://dx.doi.org/10.2147/DDDT.S13029.

[36] R. de Wit, J. de Bono, C. Sternberg, K. Fizazi, B. Tombal, C.t. Wulfing, Cabazitaxel versus abiraterone or enzalutamide in metastatic prostate cancer, N. Engl. J. Med. 381 (2019) 2506–2518, http://dx.doi.org/10.1056/NEJMoa1911206.

[37] M. Tucci, C. Zichi, C. Buttigliero, F. Vignani, G. Scaglotti, M. Di Maio, Enzalutamide-resistant castration-resistant prostate cancer: challenges and solutions, OncoTargets Therapy 11 (2018) 7353–7368, http://dx.doi.org/10.2147/OTT.S153764.

[38] S. Hamis, P. Nithiarasu, G. Powathil, What does not kill a tumour may make it stronger: in silico insights into chemotherapeutic drug resistance, J. Theoret. Biol. 454 (2018) 253–267, http://dx.doi.org/10.1016/j.jtbi.2018.06.014.

[39] J. Casciari, S. Sotirchos, R. Sutherland, Mathematical modelling of microenvironment and growth in emt6/ro multicellular tumour spheroids, Cell Prolif. 25 (1) (1992) 1–22, http://dx.doi.org/10.1111/j.1365-2184.1992.tb01433.x.

[40] T. Portz, Y. Kuang, J. Nagy, A clinical data validated mathematical model of prostate cancer growth under intermittent androgen suppression therapy, AIP Adv. 2 (2012) http://dx.doi.org/10.1063/1.3697848.

[41] B. Belderbos, S. Bins, R. van Leeuwen, E. OOmen-de Hoop, N. van der Meer, P. de Bruijn, P. Hamberg, E. Overkleeft, W. van der Deure, M. Lolkema, R. de Wit, R. Mathijssen, Influence of enzalutamide on cabazitaxel pharmacokinetics: a drug–drug interaction study in metastatic castration-resistant prostate cancer (mcrpc) patients, Clin. Cancer Res. 24 (3) (2018) 541–546, http://dx.doi.org/10.1158/1078-0432.CCR-17-2336.

[42] A. Patel, E. Gawlinskis, S. Lemieux, R. Gatenby, A cellular automaton model of early tumor growth and invasion:the effects of native tissue vascularity and increase anaerobic tumor metabolism, J. Theoret. Biol. 213 (3) (2001) 315–331, http://dx.doi.org/10.1006/jtbi.2001.2385.

[43] S.H. Au, B.D. Storey, J.C. Moore, Q. Tang, Y.-L. Chen, S. Javaid, A.F. Sarioglu, R. Sullivan, M.W. Madden, R. O'Keefe, et al., Clusters of circulating tumor cells traverse capillary-sized vessels, Proc. Natl. Acad. Sci. 113 (18) (2016) 4947–4952, http://dx.doi.org/10.1073/pnas.1524448113.

[44] K.J. Cheung, A.J. Ewald, A collective route to metastasis: Seeding by tumor cell clusters, Science 352 (6282) (2016) 167–169, http://dx.doi.org/10.1126/science.aaf6546.

[45] J. Gredell, P. Turnquist, M. Maciver, R. Pearce, Determination of diffusion and partition coefficients of propofol in rat brain tissue: Implications for studies of drug action in vitro, Br. J. Anaesthesia 93 (6) (2004) 810–817, http://dx.doi.org/10.1093/bja/aeh272.

[46] A. Anderson, A hybrid mathematical model of solid tumour invasion: the importance of cell adhesion, Math. Med. Biol. 22 (2005) 163–186, http://dx.doi.org/10.1093/imammb/dqi005.

[47] D.A. Hormuth, C.M. Phillips, C. Wu, E.A.B.F. Lima, G. Lorenzo, P.K. Jha, A.M. Jarrett, J.T. Oden, T.E. Yankeelov, Biologically-based mathematical modeling of tumor vasculature and angiogenesis via time-resolved imaging data, Cancers 13 (12) (2021) http://dx.doi.org/10.3390/cancers13123008.

[48] G. Vilanova, I. Colominas, H. Gomez, A mathematical model of tumour angiogenesis: growth, regression and regrowth, J. R. Soc. Interface 14 (2017) 20160918, http://dx.doi.org/10.1098/rsif.2016.0918.

[49] P. Colli, H. Gomez, G. Lorenzo, G. Marinoschi, A. Reali, E. Rocca, Optimal control of cytotoxic and antiangiogenic therapies on prostate cancer growth, Math. Models Methods Appl. Sci. 31 (07) (2021) 1419–1468, http://dx.doi.org/10.1142/S0218202521500299.

[50] A. Karolak, K.A. Rejniak, Micropharmacology: an in silico approach for assessing drug efficacy within a tumor tissue, Bull. Math. Biol. 81 (9) (2019) 3623–3641, http://dx.doi.org/10.1007/s11538-018-0402-x.

[51] T. Reckell, K. Nguyen, T. Phan, S. Crook, E.J. Kostelich, Y. Kuang, Modeling the synergistic properties of drugs in hormonal treatment for prostate cancer, J. Theoret. Biol. 514 (2021) 110570, http://dx.doi.org/10.1016/j.jtbi.2020.110570.

[52] M.A. Strobl, J. Gallaher, J. West, M. Robertson-Tessi, P.K. Maini, A.R. Anderson, Spatial structure impacts adaptive therapy by shaping intra-tumoral competition, Commun. Med. 2 (1) (2022) 1–18.

[53] C. Wu, G. Lorenzo, D.A. Hormuth, E.A.B.F. Lima, K.P. Slavkova, J.C. DiCarlo, J. Virostko, C.M. Phillips, D. Patt, C. Chung, T.E. Yankeelov, Integrating mechanism-based modeling with biomedical imaging to build practical digital twins for clinical oncology, Biophys. Rev. 3 (2) (2022) 021304, http://dx.doi.org/10.1063/5.0086789, arXiv:https://doi.org/10.1063/5.0086789.

[54] M. Cortesi, C. Liverani, L. Mercatali, T. Ibrahim, E. Giordano, An in-silico study of cancer cell survival and spatial distribution within a 3d microenvironment, Sci. Rep. 10 (1) (2020) 1–14, http://dx.doi.org/10.1038/s41598-020-69862-7.

[55] N. Kronik, Y. Kogan, M. Elishmereni, K. Halevi-Tobias, S. Vuk-Pavlović, Z. Agur, Predicting outcomes of prostate cancer immunotherapy by personalized mathematical models, PLoS One 5 (12) (2010) e15482, http://dx.doi.org/10.1371/journal.pone.0015482.

[56] A. Burbanks, M. Cerasuolo, L. Turner, Code to Reproduce the Results of the Paper a Hybrid Spatiotemporal Model of PCa Dynamics and Insights Into Optimal Therapeutic Strategies, Zenodo, http://dx.doi.org/10.5281/zenodo.6545987.